Lead Optimization of Influenza Virus RNA Polymerase Inhibitors Targeting PA-PB1 Interaction

Satoshi Mizuta,[a]* Hiroki Otaki,[a] Takeshi Ishikawa,[b] Juliann Nzembi Makau,[c] Tomoko Yamaguchi,[a] Takuya Fujimoto,[d] Nobuyuki Takakura,[d] Nobuki Sakauchi,[d] Shuji Kitamura,[d] Hikaru Nono,[e] Ryota Nishi,[e] Yoshimasa Tanaka,[f] Kohsuke Takeda,[g] Noriyuki Nishida,[h] and Ken Watanabe [i]*

[a] Center for Bioinformatics and Molecular Medicine, Graduate School of Biomedical Sciences, Nagasaki University, 1-14 Bunkyo, Nagasaki, 852-8521, Japan

[b] Department of Chemistry, Biotechnology, and Chemical Engineering, Graduate School of Science and Engineering, Kagoshima University, 1-21-40 Korimoto, Kagoshima 890-0065, Japan

[c] Center for Virus Research, Kenya Medical Research Institute, 54840-00200, Nairobi, Kenya

[d] Chemistry, Discovery Science, Axcelead Drug Discovery Partners, Inc., 26-1, Muraoka-Higashi 2-chome, Fujisawa, Kanagawa 251-0012, Japan

[e] School of Medicine, Nagasaki University, 1-12-4 Sakamoto, Nagasaki, 852-8523, Japan

[f] Center for Medical Innovation, Nagasaki University, 1-7-1 Sakamoto, Nagasaki, 852-8588, Japan

[g] Department of Cell Regulation, Graduate School of Biomedical Sciences, Nagasaki University, 1-14 Bunkyo, Nagasaki, 852-8521, Japan

[h] Department of Molecular Microbiology and Immunology, Graduate School of Biomedical Sciences, Nagasaki University, 1-12-4 Sakamoto, Nagasaki, 852-8523, Japan

[i] Department of Lifestyle Design, Faculty of Human Ecology, Yasuda Women's University, 6-13-1 Yasuhigashi, Asaminami ward, Hiroshima 731-0153, Japan

ABSTRACT: Influenza viruses are responsible for contagious respiratory illnesses in humans and cause seasonal epidemics and occasional pandemics worldwide. Previously, we identified a quinolinone derivative **PA-49**, which inhibited the influenza virus RNA-dependent RNA polymerase (RdRp) by targeting PA−PB1 interaction. This paper reports the structure optimization of **PA-49**, which resulted in the identification of 3-((dibenzylamino)methyl)quinolinone derivatives with more potent anti-influenza virus activity. During the optimization, the hit compound **89**, which was more active than **PA-49**, was identified. Further optimization and scaffold hopping of **89** led to the most potent compounds **100** and a 1,8-naphthyridinone derivative **118**, respectively. We conclusively determined that compounds **100** and **118** suppressed the replication of influenza virus and exhibited anti-influenza virus activity against both influenza virus types A and B in the range of $EC_{50} = 0.061–0.226$ μM with low toxicity ($CC_{50} = >10$ μM).

INTRODUCTION

Influenza A and B viruses are responsible for contagious respiratory illnesses in humans and for seasonal epidemics of influenza, causing hundreds of thousands of deaths worldwide.[1,2] The pandemic of influenza A 2009 H1N1 virus strains is caused by genetic reassortment between human, swine, and avian viruses.[3] According to the World Health Organization (WHO), a new avian-like H1N1 swine influenza virus with 2009 pandemic viral genes has been recently identified in China and poses a threat to human pandemics.[4] Although vaccination is the main preventive method against influenza virus infections, there are limitations (e.g., sustainability and cross-protection) against all subtypes of influenza viruses. Approved anti-influenza drugs are classified into three types; M2 ion-channel inhibitors (i.e., amantadine and rimantadine), neuraminidase (NA) inhibitors (i.e., zanamivir, oseltamivir, peramivir, and laninamivir), and RNA-dependent RNA polymerase (RdRp) inhibitors (favipiravir, baloxavir marboxil (BXM)) (Figure 1).[5,6] However, the influenza virus's high mutation rate causes extensive variation, which often reduces drug effects. The M2 ion-channel blockers are already not effective against currently circulating viruses.[7-9] Oseltamivir resistance among H3N2 and 2009 H1N1 seasonal viruses was also reported.[10,11] The influenza RdRp complex is an attractive target and has been given considerable attention by pharmacologists because it is essential for both transcription and replication of the viral genome. The complex comprises of three subunits (PA, PB1, and PB2); the amino acid sequence of each subunit is highly conserved among various influenza A and B viruses.[12,13] The C-terminal region of
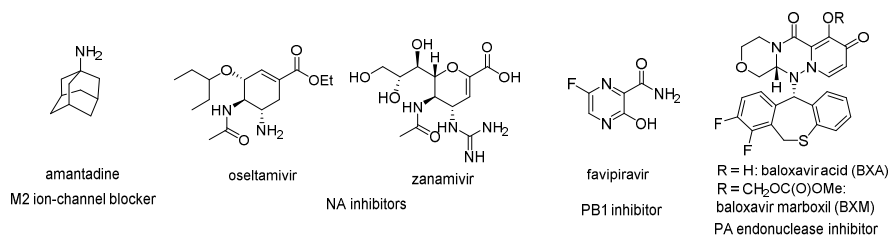
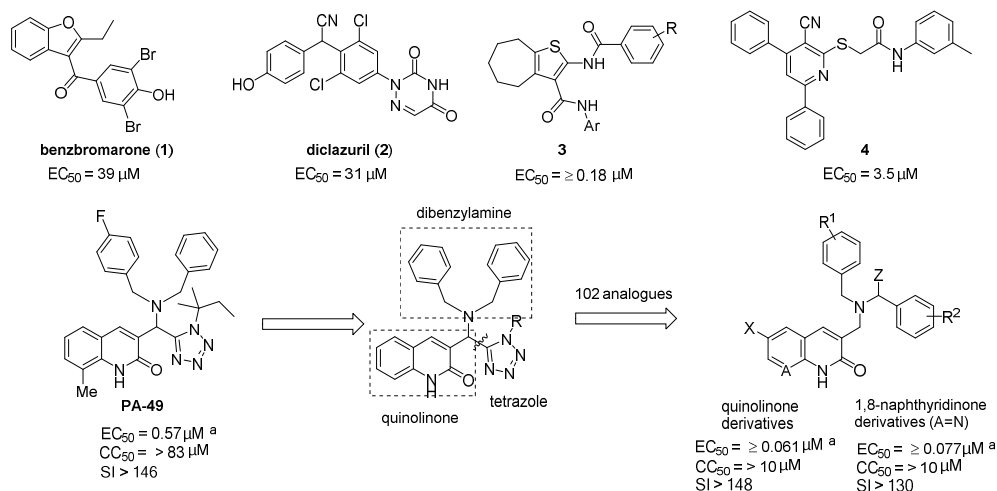**Figure 1.** Representative influenza virus inhibitors.

Figure 2. Structures of PA−PB1 subunit interaction inhibitors. [a]The EC value shows the half-maximal inhibitory concentration in crystal violet assays (see Tables 1 and 2).

PA is involved in protein-protein interaction with the N-terminal region of PB1.[14,15] The N-terminal region of the PA subunit plays a critical role in the endonuclease active site.[16] The PB1 subunit plays a role in both RNA polymerization and RNA polymerase assembly with the three protein subunits in a linear manner.[17, 18] The C-terminal region of PB1 contacts with the N-terminal region of PB2 for the RNA polymerase assembly. The region for recognizing and binding to capped RNA for generation of primers for RNA synthesis is in the PB2 subunit.[19] Therefore, RdRp inhibitors are potential targets for suppressing propagation of multiple influenza virus strains.[20] Currently, two types of RdRp inhibitors [favipiravir as a nucleic acid analog (PB1 inhibitor) and BXM as the prodrug of baloxavir acid (BXA know as PA endonuclease inhibitor)] have been approved in Japan.[21]

However, specific mutations in RdRp caused a robust reduction in susceptibility to favipiravir and BXA.[22,23] Thus, developing a new class of influenza virus inhibitors to inhibit RdRp functions through different mechanisms is required. Assembling three subunits is essential for eliciting its transcription and replication functions.[24,25] Based on the X-ray structure of the PA−PB1 complex,[13,26] various small molecules targeting PA−PB1 subunit interaction have been identified so far (Figure 2). Benzbromarone **1** and diclazuril **2** have been discovered by *in silico* screening from a chemical database including 4000 drugs.[27] Loregian and Tabarrini et al. have developed cycloheptathiophene-3-carboxamide derivatives (**3**) *via* structural optimization and structure-based drug discovery (SBDD).[28,29] 4,6-Diphenylpyridine derivative (**4**) has also been identified as a promising anti-influenza agent that disrupt PA−PB1 interaction.[30] Small molecule and small peptide inhibitors targeting the subunits interaction of the RdRp have been identified.[31-34]

We have previously discovered small molecules targeting PA–PB1 interaction using a SBDD algorithm called Nagasaki University Docking Engine.[35] Upon screening from a chemical library based on the Asinex database (600,000 compounds), we identified some virtual hit compounds with promising anti-influenza virus activities. Among them, a new chemotype of quinolinone derivative **PA-49** was the most potent inhibitor of influenza virus A/WSN/33 with 50% effective concentration (EC$_{50}$) of 0.57 μM. In this study, we performed structure optimization of **PA-49** for drug discovery. Various quinolinone derivatives were designed, synthesized, and evaluated for their anti-influenza virus activity using cell-based assay. As a result, several improved compounds that are more active than **PA-49** were successfully obtained. The amino acid sequence of PA binding to PB1 is highly conserved among various influenza virus strains, including the H1N1, H3N2, and H5N1 subtypes. The anti-influenza virus activity against both influenza virus types A and B of the highly potent compounds was evaluated by cell-based assay, and exhibited in the range of EC$_{50}$ = 0.061–0.226 μM with low toxicity (CC$_{50}$ > 10 μM). Here, we report their design and synthesis, biological evaluation, the structure-activity relationships (SARs) and the docking studies.

Results and discussion

Chemistry. We have previously reported that the hit compound **PA-49** inhibited the replication of the influenza virus targeting the PA−PB1 interaction.[35] The molecular structure is characterized by a quinolinone ring bearing a dibenzyl-aminomethyl group at α-position of methyl group of 3-methylquinolinone and a tetrazole ring at the α-position. In docking studies (Figure S5), the quinolinone ring of **PA-49** revealed the interaction with PA residue Trp706, a key residue in the hydrophobic pocket for binding PA to PB1. Their dibenzylamine moieties were located
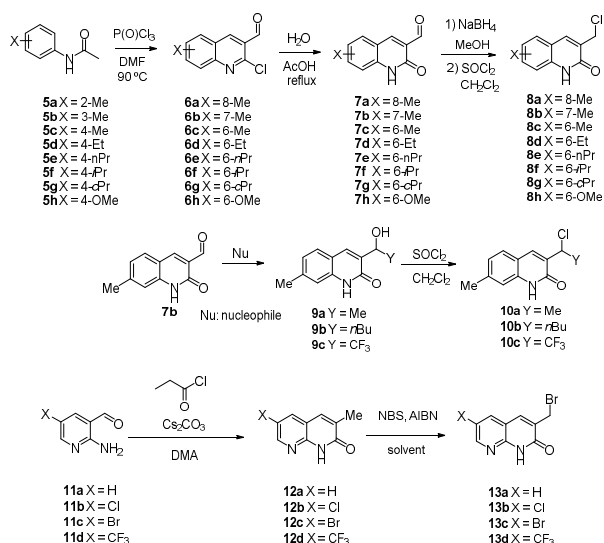
toward Leu640, and Leu666 which are required for PA-PB1 interface. However, the remarkable interaction between PA and the tetrazole ring was not observed. We thus focused on replacing the tetrazole ring as a starting point for lead optimization. First, 3-formyl-2-quinolinone derivatives (**7**) as scaffolds were synthesized according to the methodology described in the literature (Scheme 1).[36,37] The condensation of acetanilide derivatives (**5a−h**) with Vilsmeir–Haack reagents prepared from DMF and phosphoryl chloride afforded 3-formyl-2-chloroquinoline derivatives (**6a−h**); the following hydrolysis with H_2O in acetic acid led to 3-formyl-2-oxoquinoline derivatives (**7a−h**). The reduction of **7a−h** with sodium borohydride provided the corresponding alcohols which then reacted with thionyl chloride to obtain 3-chloromethyl-2-quinolinone derivatives (**8a−h**). Also, a nucleophilic addition to 3-formyl-7-methylquinolinone derivatives (**7b**) with methylmagnesium chloride (MeMgCl), *n*-butyl lithium or Ruppert reagent gave the corresponding secondary alcohols (**9a−c**). The resulting alcohols (**9a−c**) were treated with thionyl chloride, affording the corresponding chlorine-substituted derivatives (**10a−c**). 1,8-Naphthyridinone derivatives (**13a−d**) were also prepared according to the previously described method (Scheme 1).[38] The condensation of 5-substituted-2-aminonicotinaldehydes (**11a−d**) with propionyl chloride afforded 3-methyl 1,8-naphthyridinone (**12a−d**) followed by bromination with NBS and AIBN, which afforded 3-bromomethyl-1,8-qunazolidinone derivatives (**13a−d**).

Scheme 2. Synthetic Routes of Asymmetric Secondary Amine Derivatives
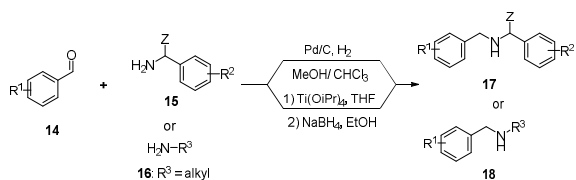

Two synthetic routes were used for the synthesis of secondary amine derivatives (Scheme 2). One is a one-step reductive amination of benzaldehydes **14** and non- or branched benzylamines (**15**) or alkylamines (**16**) with a catalytic amount of Pd/C in a mixture
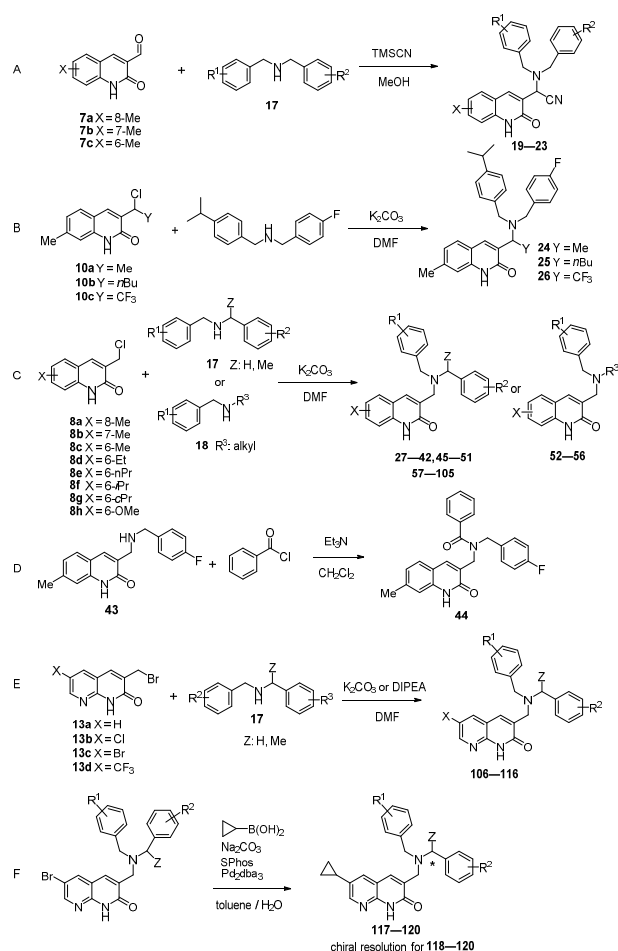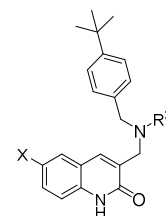
of MeOH and $CHCl_3$ under H_2 gas.[39] In another reductive amination, titanium (IV) isopropoxide was used to form imine from benzaldehydes **14** and primary amines (**15** or **16**); the following sodium borohydride reduction afforded the corresponding secondary amine.[40] Those methods enable to obtain various secondary amines: dibenzylamine derivatives (**17**) and *N*-alkyl benzylamine derivatives (**18**). Using synthesized quinolinone (**7a−h**, **8a−h**, and **10a−c**) and dibenzylamine (**17**), we started preparation of 3-methylquinolinone derivatives bearing substituents: nitrile, hydrogen and alkyl chains at the α-position of the methyl group (Scheme 3). To obtain nitrile compounds, we performed three-component coupling reactions of aldehydes (**7a−c**), dibenzylamine **17**, and trimethylsilyl cyanide to afford corresponding α-aminoacetonitliles (**19−23**), which are shown in Scheme 3A.[41] In parallel, an alkylation reaction for synthesizing **24−26** that is based on alkylation of *N*-(4-fluorobenzyl)-1-(4-isopropylphenyl)methanamine with 3-chloromethyl-2-quinolinone derivatives **10a−c** was performed (Scheme 3B). The procedure was able to access a wide range of α-amino quinolinone derivatives (**27−42** and **45−105**) *via* the amination of **8a−h** with **17** or **18** (Scheme 3C). Separately, an amide compound **44** was prepared from a monobenzyl compound **43** (Scheme 3D). The reaction of **13a−d** with **17** afforded the corresponding 1,8-naphthyridinone derivatives (**106−116**) (Scheme 3E).

Table 1. Biological Activity of a Series of Quinolinone Derivatives (PA-49, 19–91)[c]
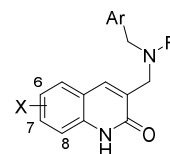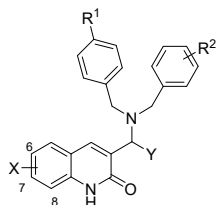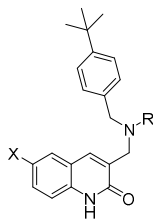

Compd	X	Y	R^1	R^2	Antiviral activity EC$_{50}$ (μM)[a]	Cytotoxicity CC$_{50}$ (μM)[b]
PA-49	8-Me	(triazole)	F	H	0.57 ± 0.02	> 83
19	8-Me	CN	F	H	38 ± 10	> 83
20	8-Me	CN	^{i}Pr	H	16 ± 2	> 83
21	7-Me	CN	^{i}Pr	H	5.6 ± 0.6	> 83
22	7-Me	CN	^{i}Pr	4-F	54 ± 0.1	21
23	6-Me	CN	^{i}Pr	H	15 ± 0.8	> 83
24	7-Me	Me	^{i}Pr	4-F	1.9 ± 0.2	> 33
25	7-Me	nBu	^{i}Pr	4-F	N.D.	> 33
26	7-Me	CF$_3$	^{i}Pr	4-F	N.D.	> 33
27	7-Me	H	^{i}Pr	4-F	2.0 ± 0.4	> 33
28	7-Me	H	^{i}Pr	4-Cl	6.1 ± 1.3	> 33
29	7-Me	H	^{i}Pr	2-F	1.8 ± 0.1	> 33
30	7-Me	H	^{i}Pr	3-F	2.1 ± 0.7	> 33
31	7-Me	H	Cl	4-Cl	N.D.	> 33
32	7-Me	H	^{t}Bu	4-F	1.6 ± 0.1	> 33
33	7-Me	H	Et	4-F	1.8 ± 0.1	> 33
34	7-Me	H	CF$_3$	4-F	2.1 ± 0.1	> 33
35	7-Me	H	^{t}Bu	3,5-2F	3.5 ± 1.0	> 33
36	6-Me	H	^{t}Bu	H	0.92 ± 0.04	> 5.0
37	6-Me	H	^{t}Bu	4-F	0.39 ± 0.13	> 27
38	8-Me	H	^{t}Bu	4-F	1.8 ± 0.0	N.D.
39	6-Et	H	^{t}Bu	4-F	0.64 ± 0.05	> 33
40	6-Et	H	^{t}Bu	3,4-2F	6.5 ± 0.5	> 33
41	6-nPr	H	^{t}Bu	4-F	28 ± 5	8.4
42	6-^{i}Pr	H	^{t}Bu	4-F	1.9 ± 0.1	7.9

Compd	X	Ar	R	Antiviral activity EC$_{50}$ (μM)[a]	Cytotoxicity CC$_{50}$ (μM)[b]
43	7-Me	(4-F-phenyl)	H	N.D.	> 33
44	7-Me	(4-F-phenyl)	(benzoyl)	N.D.	> 33
45	6-Et	(naphthyl)	(4-F-benzyl)	2.1 ± 0.0	> 5.0
46	6-Me	(naphthyl)	(3-F-phenethyl)	3.1 ± 0.8	> 5.0
47	6-Et	(naphthyl)	(3-F-phenethyl)	4.1 ± 0.4	> 5.0
48	6-Me	(biphenyl)	(4-F-benzyl)	N.D.	> 5.0
49	6-Et	(biphenyl)	(4-F-benzyl)	N.D.	> 5.0
50	6-Me	(naphthyl)	(4-F-benzyl)	1.8 ± 0.2	> 5.0
51	6-Et	(naphthyl)	(4-F-benzyl)	N.D.	> 5.0

Compd	X	R^3	Antiviral activity EC$_{50}$ (μM)[a]	Cytotoxicity CC$_{50}$ (μM)[b]
52	7-Me	(cyclopentyl)	N.D.	> 10
53	7-Et	(cyclopentyl)	N.D.	9.0
54	7-Me	(cyclohexylmethyl)	1.9 ± 0.1	> 10
55	6-Me	(hydroxypropyl)	N.D.	> 10
56	6-Me	(hydroxybutyl)	N.D.	> 10

Table 1. continued

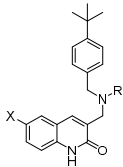| Compd	X	R	Antiviral activity EC$_{50}$ (μM)^a	Cytotoxicity CC$_{50}$ (μM)^b	Compd	X	R	Antiviral activity EC$_{50}$ (μM)^a	Cytotoxicity CC$_{50}$ (μM)^b
57	Me	—OCH$_2$OMe	0.38 ± 0.08	6.4	75	Me	—SCF$_3$	1.3 ± 0.2	> 5.0
58	Et	—OCH$_2$OMe	1.0 ± 0.2	> 10	76	Me	—CN	0.50 ± 0.08	> 5.0
59	Me	—OH	2.1 ± 0.1	4.9	77	Me	—SCF$_2$H	0.65 ± 0.39	> 5.0
60	Et	—OH	1.8 ± 0.1	> 10	78	Me	HO— (benzyl)	N.D.	> 10
61	Me	—O—CO$_2$tBu	1.8 ± 0.0	> 10	79	Et	HO— (benzyl)	N.D.	> 10
62	Me	—O—CO$_2$H	2.7 ± 0.9	> 10	80	Me	Me, —F	1.3 ± 0.9	> 33
63	Me	—OMe	0.33 ± 0.12	> 10	81	Et	Me, —F	0.52 ± 0.16	2.8
64	Me	—OEt	0.54 ± 0.09	> 10	82	^{i}Pr	Me, —F	5.4 ± 0.7	13.1
65	Me	—O—iPr	1.5 ± 1.8	> 5.0	83	Me	Me, —F	0.50 ± 0.02	> 5.0
66	Me	—O—propyl	3.0 ± 0.7	> 5.0	84	Et	Me, —F	0.79 ± 0.11	> 5.0
67	Me	—O—ethyl	N.D.	> 5.0	85	Me	Me, —F	N.D.	> 5.0
68	Me	—C(O)NH$_2$	N.D.	> 5.0	86	Et	Me, —F	N.D.	> 5.0
69	Me	—O—CH$_2$CH$_2$OH	N.D.	> 5.0	87	Me	Me, —OMe	0.26 ± 0.03	> 5.0
70	Me	—OCF$_3$	0.49 ± 0.02	> 5.0	88	Et	Me, —OMe	0.22 ± 0.01	> 5.0
71	Me	—OCF$_2$H	0.27 ± 0.07	> 5.0	89	Et	Me, —OMe	0.103 ± 0.0016	> 5.0
72	Et	—OCF$_2$H	0.46 ± 0.01	> 5.0	90	Me	Me, —OCF$_2$H	0.36 ± 0.23	> 5.0
73	Me	—SMe	0.51 ± 0.12	> 5.0	91	Et	Me, —OCF$_2$H	0.32 ± 0.09	> 5.0
74	Me	—NMe$_2$	0.46 ± 0.00	> 5.0					

^{a}50% effective concentration against the A/WSN/33 virus determined by CV staining. ^{b}50% cytotoxic concentration for Madin–Darby canine kidney (MDCK) cells measured using the CV assay. ^{c}EC$_{50}$ values were calculated from two or three independent experiments. N.D., not determined.
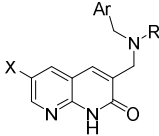
For the synthesis of compounds (**117−120**), we executed further transformation of 6-bromo-1,8-naphthyridinone derivatives by using a Suzuki-Miyaura cross-coupling reaction with cyclopropyl boronic acid (Scheme 3F). With respect to compounds (**118−120**), the synthesized racemates were separated by chiral column chromatography to obtain the chiral isomers (**118−120**).

Biological Evaluation. PA-49 consists of N-(α-substituted methylene)dibenzylamine and a tetrazole ring bearing at the same α-position of methyl group of 3-methylquinolinone. Since the quinolinone ring is a privileged scaffold found in many biological compounds,[42,43] we mainly focused on the derivatization by modifying the tetrazole ring and dibenzylamino groups with keeping structure of quinolinone. We synthesized a series of quinolinone analogs and determined their EC$_{50}$values against the A/WSN/33 virus in infected Madin–Darby canine kidney (MDCK) cells using crystal violet (CV) assay.[44] Cytotoxicity to uninfected MDCK cells was evaluated in parallel (Table 1). **PA-49** showed a promising antiviral activity (EC$_{50}$ = 0.57 μM) and appreciable cytotoxicity (EC$_{50}$ = >83 μM). During the initial modification, the replacing of tetrazole ring for other substitutes: nitrile, methyl, n-butyl, CF$_3$, and hydrogen were addressed (**19–27**). Among them, **24** and

Table 2. Biological Activity of a Series of Quinolinones (92−105) and 1,8-Naphthyridinone Derivatives (106−120)[C]

Compd	X	R	Antiviral activity $EC_{50}(\mu M)^a$	Cytotoxicity CC_{50} $(\mu M)^b$
92	Me		0.22 ± 0.01	> 10
93	Me		0.12 ± 0.01	9.8
94	OMe		0.12 ± 0.01	4.1
95	OMe		0.46 ± 0.01	8.5
96	^{i}Pr		0.68 ± 0.22	> 10
97	^{i}Pr		0.48 ± 0.01	> 10
98	Me		0.11 ± 0.03	> 10
99	Et		0.17 ± 0.05	> 10
100	OMe		0.061 ± 0.007	> 10
101			0.069 ± 0.002	> 10
102			0.090 ± 0.016	> 10
103			1.2 ± 0.3	> 10
104	OMe		0.085 ± 0.018	> 10
105			0.63 ± 0.01	> 10

Compd	X	Ar	R	$[\alpha]_D^{30}(°)$ CHCl$_3$	Antiviral activity $EC_{50}(\mu M)^a$	Cytotoxicity CC_{50} $(\mu M)^b$
106	H	^{t}Bu	OMe	–	N.D.	1.8
107	H	^{t}Bu	OMe	–	N.D.	1.8
108	H	OCF$_3$	OMe	–	1.9 ± 0.2	> 10
109	Cl	OCF$_3$	OMe	–	3.6 ± 0.0	> 10
110	Cl	^{t}Bu	NMe$_2$	–	1.5 ± 0.5	> 10
111	Br	^{t}Bu	NMe$_2$	–	0.53 ± 0.07	> 10
112	Br	^{t}Bu	NMe$_2$	–	0.10 ± 0.01	6.1
113	Br	OCF$_3$	NMe$_2$	–	N.D.	4.7
114	Br	^{t}Bu	OMe	–	0.53 ± 0.01	> 10
115	Br	^{t}Bu	OCF$_3$	–	0.28 ± 0.00	> 10
116	CF$_3$	^{t}Bu	OCF$_3$	-100.5	0.26 ± 0.01	> 10
117		^{t}Bu	OMe	-154.0	0.16 ± 0.06	> 10
118		^{t}Bu	OCF$_3$	-102.4	0.077 ± 0.014	> 10
119		^{t}Bu	OCF$_3$	-124.4	2.01 ± 0.06	N.D.
120		CF$_3$	OCF$_3$	−83.5	0.12 ± 0.02	7.9

^{a}50% effective concentration against the A/WSN/33 virus determined by CV staining. ^{b}50% cytotoxic concentration for Madin–Darby canine kidney (MDCK) cells measured using the CV assay. ^{c}EC$_{50}$ values were calculated from two or three independent experiments. N.D., not determined.

27 with the small size of α-substituent such as hydrogen and methyl group showed a more potent anti-influenza activity (EC$_{50}$ = 1.9 or 2.0 μM) than those of compounds 22, 25, and 26 bearing nitrile, CF$_3$, and n-butyl at the α-position (EC$_{50}$ = >5.4 μM). Further structure modifications were focused on the *para*-substituted group on one of two phenyl rings in dibenzylamino group of 3-(methylene)quinolinone derivatives. The introduction of ethyl, isopropyl, *tert*-butyl, and CF$_3$ at *para*-positions indicated promising antiviral activities (27, 32−34) in which (4-*tert*-butyl)benzyl-(4-fluorobenzyl)amine derivative 32 afforded EC$_{50}$ = 1.6 μM. Regarding the methyl group on the quinolinone ring, 6-methyl analogue (37) exhibited the most potent activity than 7-methyl analogue (32) and 8-methyl analogue (38). In comparison with the substitute at the 6-position, methyl and ethyl groups revealed higher antiviral activity than propyl and isopropyl groups (37, 39

vs 41, 42). In deed, the EC$_{50}$ values for 37 and 39 were 0.39 and 0.64 μM, and those for 41 and 42 were 28 and 1.9 μM, respectively.

Monobenzyl derivative 43 and the amide derivative 44 were inactive against influenza A virus. Derivatives (45−51) having naphthyl or biphenyl ring were synthesized; however, they exhibited lower activity by comparison with the corresponding derivatives having 4-*tert*-butylphenyl (37 vs 48, 50 and 39 vs 45, 49, 51). These results suggested the 4-*tert*-butylphenyl group served as an efficient side chain for anti-influenza virus activity. The introduction of cyclopentyl and aliphatic chain: cyclohexylmethyl and hydroxypropyl (52−56) resulted in the lack and unsatisfied inhibitory activity (37 vs 52, 54, 55 and 39 vs 53, 56).

Considering importance of the 4-*tert*-butylphenyl group of dibenzylamine moiety in compounds 37 and 39, we explored a
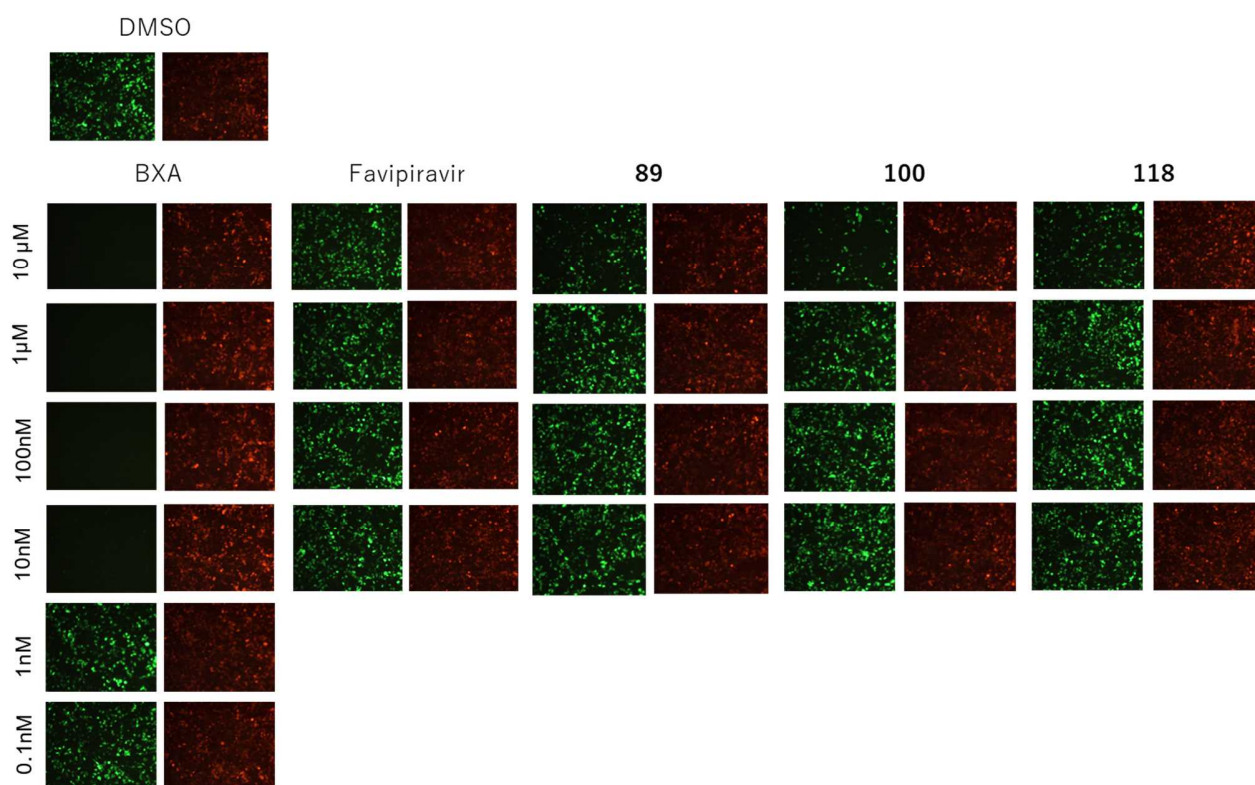
Figure 3. Inhibitory effects of compounds **89**, **100**, and **118** on the influenza virus RdRp activity. 293T cells were co-transfected with the viral protein expression plasmids (pCAGGS-PA-WSN, pCAGGS-PB1-WSN, pCAGGS-PB2-WSN, and pCAGGS-NP-WSN), model viral genome expression plasmid [pPolI/NP(0)GFP(0)], and control plasmid pDsRed2-monomer-N1. Two hours after transfection, 10-fold serially diluted compounds (10 μM−0.1 nM for BXA, 10 μM−10 nM for favipiravir, **89**, **100** and **118**) were added, and then incubated for 22 h. Two independent experiments were performed and representative data is shown. The represent images of cells observed by fluorescence microscopy are shown at the green (GFP) and red (DsRed2) channels.
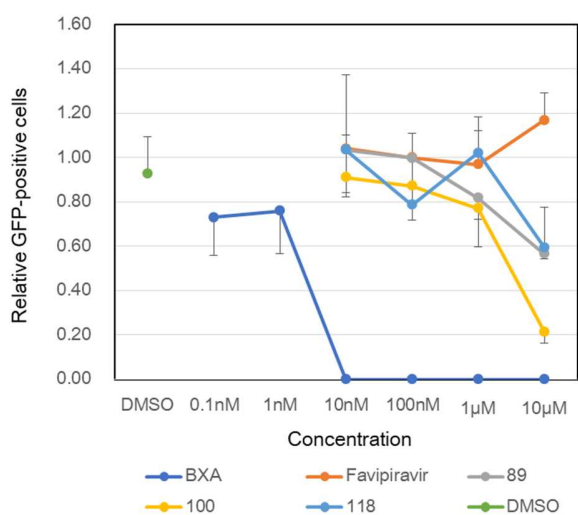

Figure 4. Relative GFP-positive cell number is estimated as the ratio of the number of GFP-positive to DsRed-positive cells from experiments shown in Figure 3. Means and standard deviations from there different miscopy fields are shown.

series of compounds (**57−91**) with different *para*-substituted groups other than fluorine on another phenyl ring for their anti-influenza virus activity. The alkoxyl, amide, sulfide, amino, and nitrile groups were investigated, and it was determined that compounds **63, 70,** and **71,** bearing alkoxyl group with a short carbon chain (methoxy (**63**), trifluoromethoxy (**70**), and difluoromethoxy (**71**), exhibited promising inhibitory activity. The compounds with the other substitutes such as methylsulfide (**73**), dimethylamino (**74**), and nitrile (**76**) also showed potent activity. We further examined a series of compounds (**78−93**) with branched benzyla-mines. Optically active (*R*)-2-amino-2-phenylethan-1-ol deriva-tives (**78, 79**) showed a considerable lack of activity. The remark-able difference between (*R*)-isomers and (*S*)-isomers of 2-(*para*-substituted)phenylethyl derivatives (**83−86**) was observed. (*S*)-1-(4-Fluorophenyl)ethan-1-amine derivatives (**83, 84**) exhibited exactly anti-influenza virus activity compared to (*R*)-isomers (**85, 86**). This trend was also observed between (*S*)-isomer and the racemic compounds. That is, the antiviral activity of (*S*)-1-(4-methoxyphenyl)ethan-1-amine derivative (**89**) was 2 folds potent compared to those of racemic compound (**88**). These results suggested that the methyl chain of (*S*) -1-(4-substituted-phenyl)ethan-1-amine improved the antiviral activity.

Second round optimization. Further optimization of the compound **89** gave us two important insights into biological effec-tiveness (Table 2). From the antiviral activity of a series of quino-
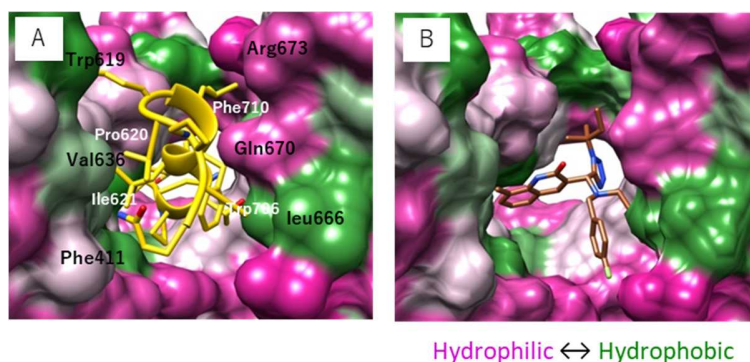
Hydrophilic ⟷ Hydrophobic

Figure 5. A) Crystal structure (PDB code: 2ZNL) of PA–PB1 (yellow) and the B) binding structure of **PA-49** to PA from our docking simulations. Hydrophilic (pink) and hydrophobic (green) regions of PA are illustrated with some key PA residues.
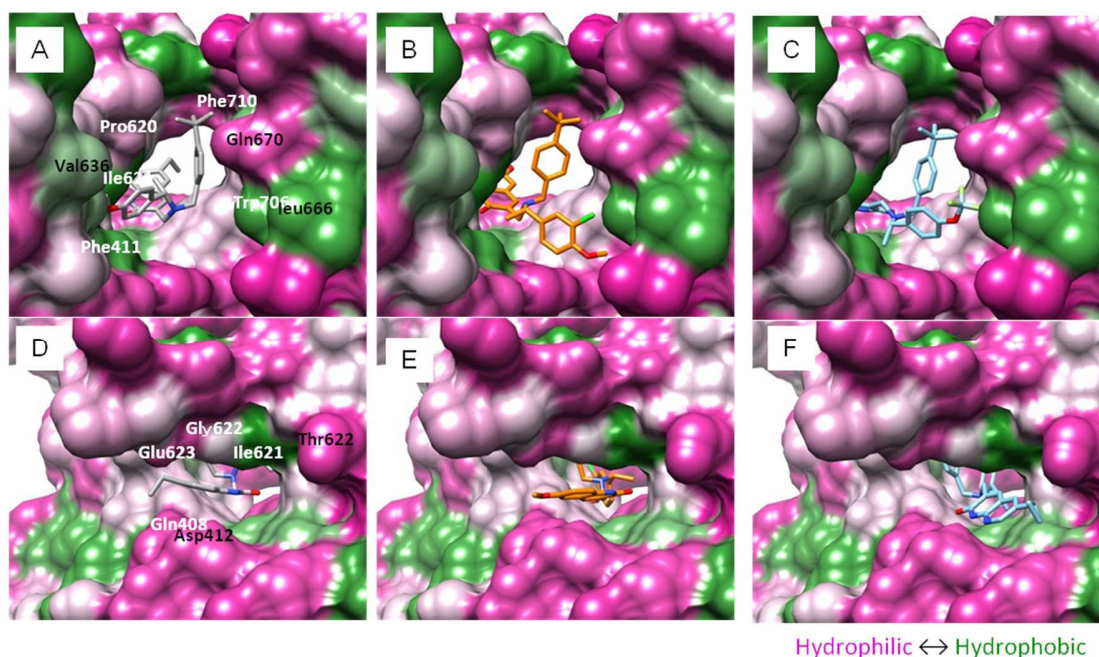

Hydrophilic ⟷ Hydrophobic

Figure 6. Docking orientations of compounds **89** (A, D), **100** (B, E), and **118** (C, F) in the PA cavity based on the crystal structure (PDB code: 2ZNL). The views (D–F) visualize the interaction of quinolinone unit for **89**, **100**, and 1,8-naphthyridinone unit for **118**.

linones (**92−105**), the first insight is that the insertion of a chlorine atom at the meta-position on the para-substituted phenyl ring improved the potency compared to the hydrogen atom at the meta-position (**74** vs **92**, **87** vs **98**, **88** vs **99**). Another insight is that among analogues (**98−101**), compound (**100, 101**) bearing methoxy and cyclopropyl groups at the 6-position of quinolinone ring had the larger potency compared to the compounds (**98, 99**) with methyl, ethyl groups.

Finally, we identified the most potent compounds **100** and **101** with beneficial characters, which exhibited EC_{50} = 0.061 and 0.069 μM respectively, with low cytotoxicity (CC_{50} = >10 μM). Aiming at scaffold hopping,[45] SARs of compounds (**106−120**) with a 1,8-naphthyridinone core were synthesized, and then their EC_{50} values were determined using the CV assay. Compounds (**106, 107**) showed their cytotoxicity without anti-influenza virus activity. Compounds (**111**) with bromine substitute at the 6-position of 1,8-naphthyridinone ring exhibited better inhibitory activity than compound (**110**) with chlorine substitute. A promis-

ing inhibitory effect was observed in 1-(4-alkoxyphenyl)ethan-1-amine derivatives (**114−118** and **120**). Among them, the chiral 1-(4-trifluoromethoxyphenyl)ethan-1-amine derivative (**118**) bearing cyclopropyl group at the 6-position of 1,8-naphthyridinone exhibited the best potency at inhibiting influenza viruses. The anti-influenza virus activity of (−)-isomer **118** was higher than that of (+)-isomer **119**; each EC_{50} value showed with 0.077 and 2.0 μM, respectively. This result that the methyl chain of (S)-1-(4-substituted-phenyl)ethan-1-amine improved the antiviral activity would be consistent with SARs for quinolinones derivatives as shown in Table 1. Consequently, the absolute configuration of (S)-**118** was expected. In addition, the $[\alpha]_D^{30}$ values of **116** and **117** with S configuration were −100.5 and −154.0, respectively; the sign of the optical rotation is consistent with that of (−)-**118**.

Transcription assay. We synthesized a set of 3-((dibenzylamino)methyl)quinolinone derivatives in the first round of optimization of compound **PA-49**. After testing the compounds

```
A/Virginia/24/2009 (H1N1)      KC781932    601
A/Quebec/147365/2009 (H1N1)    FN434450    SVKEKDMTKEFFENKSETWPIGESPRGVEEGSIGKVCRTLLAKSVFNSLY
A/WSN/33(H1N1)                 X17336      SVKEKDMTKEFFENKSETWPIGESPRGVEEGSIGKVCRTLLAKSVFNSLY
A/PR8/34(H1N1)                 EF467820    SVKEKDMTKEFFENKSETWPVGESPKGVEEGSIGKVCRTLLAKSVFNSLY
A/Aichi/2/68 (H3N2)            CY121122    SVKEKDMTKEFFENKSETWPIGESPKGVEESSIGKVCRTLLAKSVFNSLY
A/HongKong/156/97(H5N1)        AJ289874    SVKEKDMTKEFFENKSETWPIGESPKGVEDGSIGKVCRTLLAKSVFNSLY
                                           SIKEKDMTKEFFENRSETWPIGESPKGVEEGSIGKVCRTLLAKSVFNSLY
                                           *:***********:****:****:***:.*****************

651                                        701        716
ASPQLEGFSAESRKLLLIVQALRDNLEPGTFDLGGLYEAIEECLINDPWV    LLNASWFNSFLTHALK
ASPQLEGFSAESRKLLLIVQALRDNLEPGTFDLGGVYEAIEECLINDPWV    LLNASWFNSFLTHALK
ASPQLEGFSAESRKLLLIVQALRDNLEPGTFDLGGLYEAIEECLINDPWV    LLNASWFNSFLTHALR
ASPQLEGFSAESRKLLLIVQALRDNLEPGTFDLGGLYEAIEECLINDPWV    LLNASWFNSFLTHALS
ASPQLEGFSAESRKLLLVVQALRDNLEPGTFDLEGLYEAIEECLINDPWV    LLNASWFNSFLTHALR
SSPQLEGFSAESRKLLLIVQALRDNLEPGTFDLEGLYGAIEECLINDPWV    LLNASWFNSFLTHALR
:**************:***********.*:*.***********           *****:*******
```

Figure 7. Amino acid sequence alignment of influenza virus PA protein residues 601–716 of H1N1, H3N2 and H5N1 subtypes indicating residues (labelled with red) that are required for PA–PB1 interface.

Table 3. Effective Activity of Compounds 100 and 118 against Multiple Influenza Strains

Strain	Subtype	Compound EC$_{50}$ (μM)[a]				
		100	**118**	Oseltamivir phosphate	Favipiravir	Baloxavir acid
A/WSN/33	H1N1	0.061 ± 0.01	0.077 ± 0.01	2.01± 0.82	1.9 ± 0.2	0.003 ± 0.01
A/Puerto Rico/8/34	H1N1	0.072 ± 0.02	0.067± 0.02	11.6± 6.8	N.D.	0.007± 0.00
A/Virginia/ATCC2/2009[b]	H1N1	0.077 ± 0.02	0.064 ± 0.01	18.5 ± 6.21	N.D.	0.006± 0.01
A/California/7/2009[b]	H1N1	0.23± 0.08	0.27 ± 0.09	4.62 ± 2.28	2.9 ± 0.5	0.004 ± 0.00
A/Aichi/8/68	H3N2	0.085 ± 0.02	0.072 ± 0.02	2.25 ± 1.63	N.D.	0.004 ± 0.00
B/Lee/40	Type B	0.079 ± 0.01	0.23 ± 0.001	N.D.	N.D.	0.17 ± 0.05

[a]EC$_{50}$; 50% effective concentration estimated by the CV assay. [b]Clinical isolate of A(H1N1)pdm09 influenza. N.D., not determined. EC$_{50}$ values were calculated from three independent experiments.

for their anti-influenza virus activities, we identified **89**, **100**, and **118** as the most potent derivative of this set. To explore the inhibitory effects of compounds **89**, **100**, and **118** against RdRp activity, we performed a transcription assay (Figure 3).[46] 293T cells were cotransfected with plasmids expressing RdRp and a viral genome expressing plasmid (pPolI/NP(0)GFP(0)) encoding fluorescent protein (GFP), as a reporter. The viral genome RNA encoding GFP gene is transcribed from pPolI/NP(0)GFP(0) by cellular RNA polymerase I (pol I) and then GFP gene is transcribed by viral RdRp. Therefore, the fluorescence intensity of expressed GFP correlates with the inhibitory effect of compounds on the RdRp activity. To confirm specific inhibition of compounds against RdRp activity, a cellular RNA polymerase II (polII)-driven control vector for the expression of DsRed2 fluorescent protein, pDsRed2-monomer-N1, was also cotransfected.

Upon the treatment with **PA-49** and compound **89**, the ability to suppress viral RdRp activity was clearly observed at different concentrations (10 and 40 μM) in a dose-dependent manner (See, Supporting Information Figure S4). In contrast, oseltamivir did not decrease the intensity of green fluorescence because its target is NA. Subsequent transcription assay was conducted to compare the inhibitory effect of compounds **89**, **100**, and **118** with favipiravir and BXA (Figure 3). Figure 4 is shown as the ratio of the number of GFP-positive to DsRed-positive cells in the compound treated cells in a dose-dependent manner. When the intensity of green fluorescence derived from GFP in cells treated with 10 nM to 10 μM were examined, the reduction of green fluorescence was specifically observed at 10 μM with compounds **89**, **100**, and **118**. Although the inhibitory effect of BXA could be observed even at 10 nM, compounds **89**, **100**, and **118** exhibited higher potency compared to favipiravir. Regardless of addition of any drugs, the intensity of red fluorescence derived from DsRed2 was almost the same as that of the control (DMSO). Overall, the RdRp-mediated genome transcription may be inhibited by suppression of the PA−PB1 complex formation in the presence of **PA-49** and com-

pounds **89**, **100**, and **118**. Detailed mechanistic studies to elucidate binding mode of compounds **89**, **100**, and **118** are ongoing.

The crystal structure of the PA–PB1 complex (PDB code: 2ZNL)[13] was resolved (Figure 5A). Based on the complex structures, Liu et al. have identified the binding hot spots in the interactions of PA and PB1 complex through the molecular dynamics simulation.[26,47] For binding PA to PB1, residues; 618–621, Glu623, Val636, Leu640, Leu666, Gln670, Arg673, Trp706, and Phe710 reveal the PA–PB1 interface. In addition, the existence of three pockets in this PA cavity is important for PA binding to PB1. Residues Trp706 and Phe411 are involved in the first hydrophobic pocket. Phe710 and Leu666 contribute to form the second hydrophobic pocket. The third pocket involves Leu640 and residues 619−623. Previously identified hit compound **PA-49** showed a promising antiviral activity (EC$_{50}$ = 0.57 μM) against the A/WSN/33 virus and appreciable cytotoxicity (EC$_{50}$ = >83 μM). We performed the docking simulation of small molecule **PA-49** with PA using AMBER ff99SB and GAFF force fields (Figure 5B).[35] The binding mode revealed that quinolinone ring fitted Trp706 through π–π interactions and the isobutyl group in the tetrazole ring was in the hydrophobic pocket involving Trp706 and Phe411.

To gain insight into the binding mode of compounds **89**, **100**, and **118**, we calculated energy minimization between PA residues by using the Molecular Operating Environment (MOE) software which can be used for docking study of peptides and small molecules.[48] The most favorable docking orientations for PA and compounds **89**, **100**, and **118** are shown in Figure 6. As shown in Figures 6A–C, the bulky and hydrophobic *tert*-butylphenyl group is located in the first hydrophobic pocket generated by Trp706, Phe411. While the key interaction with the *para*-alkoxyphenyl group was not observed in **89**, **100**, and **118**, it seems to be a lot of flexibly in the PA cavity (See, Supporting Information Figure S5). 4-Methoxyphenyl group of **89** located in the vicinity of Ile621 and Val636. The *meta*-chloro substitute on 4-methoxy phenyl group of **100** was oriented toward Gly622. The trifluoromethoxy group of **118** was oriented toward Ile621 and Leu666.

As shown in Tables 1 and 2, the introduction of methyl chain with *S* configuration in the (S)-2-*para*-alkoxyphenylethyl group improved the ability to inhibit influenza virus. We assumed that the methyl chain controlled the geometry of compounds. This may produce orientation that binds well to PA. In contrast, the quinolinone and 1,8-naphthyridinone ring anchored in the third pocket involve Leu640 and residues 619−623. The quinolinone unit for **89** interacted with Gly622 through arene–cation interaction (Figure 6D). The hydrogen bonding between the oxygen of the quinolinone of **100** and Thr639 was observed (Figure 6E). The surface of the 1,8-naphthyridinone ring for **118** was an inversion of the quinolinone ring in **89** and **100**. The two nitrogen atoms of the 1,8-naphthyridinone ring oriented toward Gln408 and Asp412 (Figure 6F). In these studies, the compounds **89**, **100**, and **118** revealed the common interaction with Trp706 and Phe411. It is known that Trp706 and Phe411 are key residues of hydrophobic pocket for binding PA to PB1. Their dibenzylamine moieties were located towards Ile621, Gly622, Leu666, or Val636 which are required for a part of PA-PB1 interface. The quinolinone and 1,8-naphthyridinone rings were localized in the third pocket involving Leu640 and residues 619−623. Besides, the quinolinone ring for **100** and 1,8-naphthyridinone ring interacted with Thr639 and Gln408, respectively, through hydrogen bonding. Due to the binding mode of compounds **89**, **100**, and **118**, they might show the potent activity by competing with PB1 to disturb the PA-PB1 interactions.

As previously shown,[35] amino sequence alignment of influenza virus PA protein (residues 601–716) of H1N1, H3N2 and H5N1 subtypes are highly conserved (Figure 7). Among the subtypes, residues; 618–621, Glu623, Val636, Leu640, Leu666, Gln670, Arg673, Trp706, and Phe710, revealed on the PA−PB1 interface are also highly homologous. Because the amino acid region of influenza viruses' PA bound to PB1 is highly conserved, we hypothesized that the quinolinone derivatives **100** and 1,8-naphthyridinone derivative **118** have antiviral potency against multiple type influenza strains. Thus their antiviral activities against multiple type A influenza strains, including clinical isolates (H1N1pdm) and B, was evaluated (Table 3). The EC$_{50}$ values of compounds **100** and **118** against A/Puerto Rico/8/34 (H1N1), clinical isolates [A/Virginia/ATCC2/2009(H1N1) and A/California/7/2009(H1N1)], A/Aichi/8/68 (H3N2) and type B (B/Lee/40) viruses were in the range of 0.064–0.27 μM. The EC$_{50}$ value of oseltamivir against multiple influenza A strains showed in the range of 2.0–18.5 μM, of which the EC$_{50}$ values against A/WSN/33 and A/Puerto Rico/8/34 (H1N1) are similar to that reported previously.[44] Of note, the EC$_{50}$ value against pandemic (H1N1pdm) clinical isolates (A/Virginia/ATCC2/2009 and A/California/7/2009) were much lower than those of oseltamivir and favipiravir. Meanwhile, Cap-dependent endonuclease inhibitor BXA inhibited in the low-nanomolar range against influenza type A viruses. The effect against B/Lee/40 was similar to those of compounds **100** and **118**. Their inhibitory activities against oseltamivir- resistant A/California/7/2009(H1N1) virus were preliminarily determined to be effective (Figure S8). Taken together, identified compounds **100** and **118** may be useful as lead compounds to develop anti-influenza viral drugs targeting the PA-PB1 complex.

Conclusions

Among the limited number of classes of anti-influenza drugs, the influenza virus RdRp is an attractive drug target because RdRp is essential for the transcription and replication of the viral genome. Moreover, the amino acid sequence is highly conserved among various influenza viruses. RdRp inhibitors have high potency against multiple strains of the influenza virus. However, the newly licensed cap-dependent endonuclease inhibitor (BMB) has a low barrier to resistance due to the presence of major pathway of the PA I38T substitution.[22] We have studied the development of RdRp inhibitors with different action mechanisms. We recently identified a small molecule **PA-49** that can disrupt viral polymerase activity targeting PA–PB1 interaction. The molecular structure is characterized by three parts: quinolinone ring, dibenzylamine, and tetrazole ring. In this study, we performed structural optimization by mainly modifying the dibenzylamine moiety. Compounds (**19–91**) were synthesized and bioassayed *in vitro* to determine their inhibitory activities against influenza viruses. The initial round of optimization provided a quinolinone derivative **89** with an improved EC$_{50}$ value (0.103 μM) compared to **PA-49** (EC$_{50}$ = 0.54 μM). A transcription assay observed an inhibitory effect of viral polymerase activity of **89** and **PA-49**. The successive optimization of compound **89** afforded the most potent quinolinone derivative **100** and 1,8-naphthyridinone derivative **118** with EC$_{50}$ values of 0.061 μM, and 0.077 μM, respectively. The binding modes of **89**, **100**, and **118** to the PA were analyzed by the MOE software. Docking studies indicated that the bulky and hydrophobic *tert*-butyl group at the *para*-position of compounds mainly interacted with the first hydrophobic pocket generated by Trp706, Phe411 in the PA cavity. The quinolinone unit for **89**, **100**, and 1,8-naphthyridinone unit for **118** anchored in the third

pocket involving Leu640 and residues 619−623. The introduction of methyl chain with (S)-configuration of the 2-para-alkoxyphenylethyl group improved the ability to inhibit the replication of influenza virus. This effect may be caused by controlling the geometry of compounds. From the docking simulation, we assume that compounds competed with PB1 to suppress the PA-PB1 interaction. Further investigations to elucidate the mode of action are ongoing.

For this, the antiviral activity of compounds **100** and **118** was studied against multiple-influenza A virus strains, including clinical isolates (H1N1pdm), and against influenza B virus. Compounds **100** and **118** successfully exhibited the anti-influenza virus activity against both in the range of $EC_{50} = 0.061$–0.226 μM with low toxicity ($CC_{50} > 10$ μM). In conclusion, we performed additional structural optimization from compound **89**, which afforded improved quinolinone derivatives **100** and 1,8-naphthyridinone derivative **118** with low cytotoxicity.

Experimental Section

Materials for biological tests: MDCK cells were maintained in a minimum essential medium (MEM) purchased from Wako Pure Chemical Industries, Ltd. (Tokyo, Japan) and supplemented with 5% fetal bovine serum (FBS) from Life Technologies (Scoresby, Australia), 100 units/mL of penicillin, and 100 μg/mL of streptomycin (Nacalai Tesque Inc., Kyoto, Japan). Human embryo kidney 293T cells were obtained from America Type Culture Collection (Manassas, VA) and maintained in Dulbecco's modified Eagle's medium (Sigma Aldrich, St Louis, MO) containing 10% FBS. These cells were maintained at 37°C in an atmosphere of 5% CO_2. Influenza viruses A/WSN/33 (H1N1), A/Puerto Rico/8/34 (H1N1), A/Virginia/ATCC2/2009 (H1N1), A/Aichi/2/68 (H3N2), and B/Lee/40 were prepared as described.[46] Allantoic fluid from embryonated eggs of A/California/7/2009 (H1N1) was obtained from Dr. Hiroshi Kido (Tokushima University). All viruses were stored at −80°C until use. Oseltamivir phosphate (F. Hoffmann-La Roche, Basel, Switzerland) was dissolved in phosphate-buffered saline at the concentration of 10 mM. BXA (Funakoshi, Co., Ltd. JP) was dissolved in DMSO at the concentration of 10 mM. All compounds were maintained at −30°C until use.

Unless noted otherwise, all starting materials and reagents were obtained from commercial suppliers and used without further purification. All chemicals were purchased from Sigma Aldrich, Nacalai Tesque, Tokyo Chemical Industry, and Wako Pure Chemical Industries and used as received. All NMR spectra were recorded on Varian 500PS spectrometers or Bruker AVANCE III (300 MHz) spectrometer. ^{1}H NMR spectra are reported as chemical shifts (δ) in parts per million (ppm) relative to the solvent peak using tetramethylsilane (^{1}H) as an internal standard. Chemical shifts (δ) are quoted in parts per million (ppm), and coupling constants (J) are measured in hertz (Hz). The following abbreviations are used to describe multiplicities s = singlet, d = doublet, t = triplet, q = quartet, quint. = quintet, sext. = sextet, sept. = septet, br = broad, m = multiplet. NMR spectra were processed in ACD/SpecManager. The purity of all compounds used in assays was determined to be ≥95% by ^{1}H NMR spectroscopy and confirmed by high-resolution mass spectrometry (HRMS) or (ESI) experiments using a DART (JMS-T100TD) instrument or using JEOL JMS-T100TD for electrospray ionization (ESI+). Alternatively, MS experiments were performed using atmospheric pressure chemical ionization (APCI) and electrospray ionization (ESI) in positive or negative ion mode (LCMS-2020). Mobile phases A and B were 0.05% trifluoroacetic acid (TFA) in water

and 0.05% TFA in MeCN, respectively. The ratio of mobile phase B was increased linearly from 5 to 90% over 0.9 min, 90% over the next 1.1 min. All reactions were performed in apparatuses with magnetic stirring under an inert atmosphere. Flash column chromatography was performed over Fuji Silysia Chemical Ltd. silica gel C60 (50–200 μm) or Purif-Pack (SI or NH, SHOKO SCIENTIFIC) using an eluent system as described for each experiment. Thin-layer chromatography was performed on TLC Silica gel 60 F_{254} aluminum sheets (Merck, Ltd.) and silica gel F_{254} glass plates (Merck). Optical rotations were measured on a JACSO P2000 and are reported as $[\alpha]_D^{30}$ value; the corresponding concentration (c) is given in g/100 mL. Preparative HPLC was performed on a Gilson Preparative HPLC system using a YMC-Actus Triart C18 column (150 mm × 20 mm ID, 5 μm, YMC). Mobile phases A and B were 10 mM ammonium bicarbonate and MeCN, respectively. The ratio of mobile phase B was increased linearly in 5−10 min.

CV assay and cytotoxicity test: The anti-influenza virus activities of the compounds were evaluated by CV(crystal violet) assay as described previously with some modifications.[44,49] To evaluate the anti-influenza virus activities, MDCK cells were seeded into 96-well plates at the density of 3.0×10^4 cells/well in 100 μL of MEM containing 5% FBS and then incubated overnight. The cells were washed with MEM vitamin and added 100 μL of the serially diluted compound, then infected the cells with 100 μL of virus solution in MEM vitamin equivalent to 100 tissue culture infectious doses $(TCID)_{50}$ for type A viruses or 30 $TCID_{50}$ for B/Lee/40. Except for A/WSN/33 and B/Lee/40, viruses were grown in the presence of trypsin. The culture plates were incubated at 37°C for 48 h, and the cells were fixed with 70% EtOH and stained with 0.5% CV. After washing with water and air drying, absorbance was measured at 560 nm on an Infinite M200 Pro plate reader (Tecan Japan Co. Ltd., Kanagawa, Japan). The MDCK cells and compound for cytotoxicity testing were prepared using the above approach except for the virus treatment. After incubation for 46–48 h, the cells were fixed with 70% EtOH and stained with 0.5% CV. After washing with water and air drying, The absorbance at 560 nm was measured on an Infinite M200 Pro plate reader. EC_{50} and CC_{50} values were calculated from the dose-response curve by linear regression analysis.

Transcription assay: 293T cells (2×10^5 cells/well) were seeded into 24-well plates and incubated overnight. The cells were transfected according to the manufacturer's instructions with the following plasmids diluted using the TransIT-293 (Mirus Bio LLC, Madison, WI) transfection reagent: 75 ng of each viral protein expression plasmid (pCAGGS-PA-WSN, pCAGGS-PB1-WSN, pCAGGS-PB2-WSN, and pCAGGS-NP-WSN), 100 ng of model viral gene expression plasmid pPolI/NP(0)GFP(0),[50] and 1 μg of pDsRed2-monomer-N1. At 2 h post-transfection, the medium was replaced with 500 μL of D-MEM containing serially diluted compounds and 25 mM Hepes (pH 7.4). The next day, the expressions of GFP and DsRed2 proteins were observed by fluorescence microscopy [AXJ-5300TPHFL, Wraymer, Inc. (Osaka, Japan)], and photographs were acquired by USB camera (SR130, Wraymer).

Docking studies: Docking studies were conducted using MOE software[49] to provide insight into the binding mode of **89**, **100**, and **118** to PA (PDB code: 2ZNL). All the calculations were performed with the AMBER10: EHT force fields, [51,52] which applies AMBER10 force field and extended Hückel theory (EHT) for biomolecules and ligands, respectively. By using the MOE software, the N atom of *terti*ary amine on inhibitors was protonated to maintain the system neutral. The first docking simulation was run with a Triangle Matcher method to generate 10,000 poses. During

this simulation, the geometry of crystal structure of PA was kept fixed, and binding energies of ligands were evaluated using the London dG scorning function.[35] Toward the top 50 poses, the subsequent energy calculation was performed with a flexible receptor modeling (induced fit) that allowed to move side chains of PA residues surrounding ligands. Docking scores (in kcal/mol) were determined by GBVI/WSA dG scorning function.[53] The docking scores of the top 10 poses were shown in Figure S6. The most stable docking poses of **89**, **100**, and **118** were shown in Figure 5.

Synthesis of 6-methyl-2-oxo-1,2-dihydroquinoline-3-carbaldehyde (7c) (method A): To a solution of *p*-acetotoluidine (2.2 g, 15 mmol) in DMF (7.0 mL) was added P(O)Cl$_3$ (15 mL, 166 mmol) dropwise at 0 °C. After stirring for 16 hrs at 90 °C, the reaction mixture was cooled to room temperature. The mixture was poured carefully into ice rock, the precipitate was filtered and washed with water, and dried under vacuum affording 2-chloro-6-methylquinoline-3-carbaldehyde. The product was dissolved in acetic acid (30 mL) and water (10 mL) and stirred at 90 °C for 12 hrs. The reaction mixture was evaporated to remove the solvent. The residue was added water, and the precipitate was filtered and washed with EtOAc/n-hexane (1: 10). The product was dried under vacuum affording the desired product (227 mg, 8% yield).^{1}H NMR (500 MHz, DMSO-d6) δ 2.34 (s, 3H), 7.27 (t, *J* = 8.6 Hz, 1H), 7.50 (dd, *J* = 2.0, 8.6 Hz, 1H), 7.70 (s, 1H), 8.42 (s, 1H), 10.2 (s, 1H), 12.2 (s, 1H).

6-Ethyl-2-oxo-1,2-dihydroquinoline-3-carbaldehyde (7d): Following the method A, the title compound was synthesized in 12% yield. ^{1}H NMR (500 MHz, DMSO-d6) δ 1.20 (t, *J* = 7.6 Hz, 3H), 2.64 (q, *J* = 7.6 Hz, 2H), 7.29 (t, *J* = 8.6 Hz, 1H), 7.53 (dd, *J* = 2.0, 8.6 Hz, 1H), 7.72 (s, 1H), 8.43 (s, 1H), 10.2 (s, 1H), 12.2 (s, 1H).

6-Methoxy-2-oxo-1,2-dihydroquinoline-3-carbaldehyde (7h): Following the method A, the title compound was synthesized in 8% yield.^{1}H NMR (500 MHz, DMSO-d6) δ 3.79 (s, 3H), 7.29−7.34 (m, 2H), 7.48 (d, *J* = 2.7 Hz, 1H), 8.45 (s, 1H), 10.2 (s, 1H), 12.1 (s, 1H); LRMS (ESI⁺): m/z: 226 [M+Na]⁺

Synthesis of 3-(hydroxymethyl)-6-methylquinolin-2(1H)-one (method B): To a suspension of 6-methyl-2-oxo-1,2-dihydroquinoline-3-carbaldehyde (95 mg, 0.51 mmol) in MeOH (5.0 mL) was added NaBH$_4$ (23 mg, 0.61 eq) at room temperature. The reaction mixture was stirred for 4 h and quenched by the addition of H$_2$O. The precipitate was filtered and washed with water, and dried under vacuum affording the desired product (87 mg, 90% yield). ^{1}H NMR (500 MHz, CDCl$_3$) δ 2.33 (s, 3H), 4.38 (d, *J* = 3.9 Hz, 2H), 5.18 (t, *J* = 5.4 Hz, 1H), 7.20 (d, *J* = 8.3 Hz, 1H), 7.27 (dd, *J* = 1.7, 8.3 Hz, 1H), 7.46 (s, 1H), 7.77 (s, 1H), 11.7 (br.s, 1H).

6-Ethyl 3-(hydroxymethyl)-quinolin-2(1H)-one: Following the method B, the title compound was synthesized in 89% yield. ^{1}H NMR (500 MHz, DMSO-d6) δ 1.19 (t, *J* = 7.6 Hz, 3H), 2.64 (q, *J*= 7.6 Hz, 2H), 4.39 (dd, *J* = 1.2, 5.4 Hz, 1H), 5.21 (t, *J* = 5.4 Hz, 1H), 7.22 (d, *J* = 8.3 Hz, 1H), 7.32 (dd, *J* = 1.7, 8.3 Hz, 1H), 7.49 (s, 1H), 7.79 (s, 1H), 11.7 (s, 1H).

3-(Hydroxymethyl)-6-methoxyquinolin-2(1H)-one: Following the method B, the title compound was synthesized in 56% yield. ^{1}H NMR (500 MHz, DMSO-d6) δ 3.78 (s, 3H), 4.39 (d, *J* = 3.9 Hz, 1H), 5.20 (t, *J* = 5.4 Hz, 1H), 7.10 (dd, *J* = 2.7, 8.8 Hz, 1H), 7.23 (d, *J* = 8.8 Hz, 1H), 7.25 (d, *J* = 2.7 Hz, 1H), 7.81 (s, 1H), 11.7 (br.s, 1H); LRMS (DART⁺): m/z: 206 [M+H]⁺

Synthesis of 3-(chloromethyl)-6-methylquinolin-2(1H)-one (8c) (method C): To a suspension of 6-methyl-2-oxo-1,2-dihydroquinoline-3-carbaldehyde (67 mg, 0.35 mmol) in dichloromethane (3.5 mL) was added SOCl$_2$ (508 µL, 7.0 mmol) at

room temperature. The reaction mixture was stirred for 10 hrs, and concentrated under vacuum affording the desired product (72 mg, 99% yield). ^{1}H NMR (500 MHz, DMSO-d6) δ 2.34 (s, 3H), 4.63 (s, 2H), 7.29 (d, *J* = 8.6 Hz, 1H), 7.35 (d, *J* = 8.4 Hz, 1H), 7.45 (s, 1H), 8.05 (s, 1H), 11.9 (s, 1H).

3-(Chloromethyl)-6-ethylquinolin-2(1H)-one (8d): Following the method B, the title compound was synthesized in 99% yield. ^{1}H NMR (500 MHz, DMSO-d6) δ 1.20 (t, *J* = 7.6 Hz, 3H), 2.64 (q, *J* = 7.6 Hz, 2H), 4.63 (s, 2H), 7.24 (d, *J* = 8.3 Hz, 1H), 7.53 (dd, *J* = 2.0, 8.3 Hz, 1H), 7.50 (s, 1H), 8.07 (s, 1H), 11.9 (s, 1H).

3-(Chloromethyl)-6-methoxyquinolin-2(1H)-one (8h): Following the method C, the title compound was synthesized in 99 yield.^{1}H NMR (500 MHz, DMSO-d6) δ 3.78 (s, 3H), 4.64 (s, 2H), 7.18 (dd, *J* = 3.0, 8.8 Hz, 1H), 7.24 (d, *J* = 2.7 Hz, 1H), 7.26 (d, *J* = 9.1 Hz, 1H), 8.06 (s, 1H), 11.9 (br.s, 1H).

3-(Bromomethyl)-1,8-naphthyridin-2(1*H*)-one (13a): To a suspension of 3-methyl-1,8-naphthyridin-2(1H)-one (320 mg, 2.0 mmol) in CCl$_4$ (20 mL) was added NBS (427 mg, 2.4 mmol). The mixture was heated at 90 °C, added AIBN (49 mg, 0.2 mmol) with stirring for 5hrs. The resulting mixture was cooled to room temperature, the bulk of CCl$_4$ was evaporated. The crude was purified by column chromatography on SiO$_2$ gel (CH$_2$Cl$_2$/MeOH = 98:2) to afford the product (155 mg, 32 % yield). **^{1}H NMR** (500 MHz, CDCl$_3$) δ 4.55 (s, 2H), 7.24−7.27 (m, 1H), 7.91 (s, 1H), 7.95 (dd, *J* = 1.8, 7.8 Hz, 1H), 8.70 (dd, *J* = 1.7, 4.9 Hz, 1H), 11.1 (br.s, 1H).

(S)-N-(4-(*tert*-Butyl)benzyl-1-(4-methoxyphenyl)ethan-1-amine: An autoclave was equipped with 4-*tert*-butylbenzaldehyde (1.0 mL, 6 mmol), (S)-1-4-(methoxyphenyl) ethylamine (738 µL, 5 mmol), 10% Pd–C (50 mg, 10 wt %) in MeOH (30 mL), and CHCl$_3$ (3 mL). The solution was hydrogenated (2 atm) at room temperature until the absorption of hydrogen ceased (10 h). After the Pd–C catalyst was filtered off, solvent was removed on a evaporator. The residue was diluted with EtOAc (50 mL) and sat. NaHCO$_3$ (30 mL), and extracted. The organic layers were washed with brine, dried over MgSO$_4$ and concentrated under vacuum. The residue was purified by column chromatography on SiO$_2$ gel (hexane-EtOAc, 4 : 1 to 2:1) to afford the product (780 mg, 53% yield). ^{1}H NMR (500 MHz, CDCl$_3$) δ 1.32 (s, 9H), 1.35 (d, *J* = 6.4Hz, 3H), 3.57 (d, *J* = 13.0 Hz, 3.62 (d, *J* = 13.0 Hz, 1H), 3.78 (q, *J* = 6.6 Hz, 1H), 3.82 (s, 3H), 6.89 (d, *J* = 8.8 Hz, 2H), 7.21 (d, *J* = 8.3 Hz, 2H), 7.28 (d, *J* = 8.8 Hz, 2H), 7.34 (d, *J* = 8.3 Hz, 2H).

N-(4-(*tert*-butyl)Benzyl)-1-(3-chloro-4-methoxyphenyl)methanamine: A round bottom flask was charged with 1-(3-chloro-4-methoxyphenyl)ethan-1-one (928 mg, 5 mmol), (4-*tert*-butyl)benzylamine (1.7 mL, 3.0 eq), Ti(OiPr)$_4$ (3 mL, 1.3 eq) and MeOH(15 mL) and allowed to stir at room temperature overnight. The reaction mixture was cooled at 0 °C and NaBH4 (380 mg, 10 mmol, 2.0 eq) was added. After stirring for 20 min, the reaction was quenched with water and extracted with EtOAc. The organic layers were washed with brine, dried over MgSO$_4$ and concentrated under vacuum. The residue was purified by column chromatography on SiO$_2$ gel (hexane-EtOAc, 4 : 1) to afford the product (420 mg, 25 % yield). ^{1}H NMR (500 MHz, CDCl$_3$) δ 1.31−1.35 (m, 12 H), 3.55 (d, *J* = 13.0 Hz, 1H), 3.61 (d, *J* = 13.1 Hz, 1H), 3.78 (q, *J* = 5.7 Hz, 1H), 3.91 (s, 3H), 6.92 (d, *J* = 8.1 Hz, 1H), 7.22−7.26 (m, 3H), 7.35 (d, *J* = 8.1 Hz, 2H), 7.40 (d, *J* = 2.2 Hz, 1H).

N-(4-(*tert*-butyl)benzyl)-1-(4-(trifluoromethyl)phenyl)ethan-1-amine: To a mixture of (4-(tert-butyl)phenyl)methanamine (4.00 g, 24.5 mmol), 1-(4-(trifluoromethoxy)phenyl)ethan-1-one (5.00 g, 24.5 mmol), and in THF (200 mL) was added Ti(OiPr)$_4$ (10.5 g, 36.8 mmol). The mixture was stirred at room temperature for 2 h. To the mixture

were added EtOH (50 mL) and NaBH$_4$ (9.27 g, 245 mmol). The mixture was stirred at room temperature for 1 h and at 60 °C for 3 h. The mixture was diluted with water and the resulting precipitate was collected by filtration on the pad of Celite. The filtrate was extracted with EtOAc. The organic layer was dried over anhydrous MgSO$_4$ and concentrated in vacuo. The residue was purified by column chromatography (NH silica gel, haxane/EtOAc = 100/0 to 10/1) to afford the product (6.86 g, 80% yield) as a colorless oil. ^{1}H NMR (300 MHz, DMSO-d_6) δ 1.23 - 1.29 (m, 12 H), 3.44 (br.s, 2 H), 3.73 (br.d, J = 6.4 Hz, 1 H), 7.14 - 7.25 (m, 2 H), 7.26 - 7.34 (m, 4H), 7.43 -7.53 (m, 2H); LRMS (ESI): m/z 352.2 [M+H]$^+$

2-[Benzyl(4-fluorobenzyl)amino]-2-(8-methyl-2-oxo-1,2-dihydroquinolin-3-yl)acetonitrile (19) (Method D): *N*-benzyl-1-(4-fluorophenyl)methanamine (69 mg, 0.32 mmol) and trimethylsilyl cyanide (40 μL, 0.32 mmol) was added to a solution of 8-methyl-2-oxo-1,2-dihydroquinoline-3-carbaldehyde (60 mg, 0.32 mmol) in 2,2,2-trifluoroethanol (1.0 mL) under ambient atmosphere. The mixture was stirred for 2 h at 60 °C, and then evaporated to remove the solvent. The residue was purified by column chromatography on SiO$_2$ gel (EtOAc-MeOH, 10:1) to afford the product (57 mg, 43% yield). ^{1}H NMR (500 MHz, CDCl$_3$) δ 3.60 (d, J = 13.7 Hz, 1H), 3.63 (d, J = 13.9 Hz, 1H), 3.98 (d, J = 13.9 Hz, 1H), 4.01 (d, J = 13.7 Hz, 1H), 5.24 (s, 1H), 6.99 (t, J = 8.6 Hz, 2H), 7.16 (t, J = 7.6 Hz, 2H), 7.37−7.46 (m, 6H), 8.04 (s, 1H), 104. (s, 1H).

2-[Benzyl(4-isopropylbenzyl)amino]-2-(8-methyl-2-oxo-1,2-dihydroquinolin-3-yl)acetonitrile (20): Following the Method D, the title compound was synthesized in 60% yield. ^{1}H NMR (500 MHz, CDCl$_3$) δ 1.21 (d, J = 6.9 Hz, 6H), 2.46 (s, 3H), 2.87 (sept, J = 6.9 Hz, 1H), 3.63 (d, J = 13.7 Hz, 1H), 3.66 (d, J = 13.9 Hz, 1H), 4.02 (d, J = 13.9 Hz, 1H), 4.06 (d, J = 13.7 Hz, 1H), 5.24 (s, 1H), 7.13−7.18 (m, 3H), 7.24 (t, J = 7.4 Hz, 2H), 7.31−7.40 (m, 5H), 7.44 (d, J = 7.9 Hz, 1H), 7.48 (t, J = 7.6 Hz, 2H), 8.06 (s, 1H), 10.6 (s, 1H).

2-(Benzyl(4-isopropylbenzyl)amino)-2-(7-methyl-2-oxo-1,2-dihydroquinolin-3-yl)acetonitrile (21): Following the Method D, the title compound was synthesized in 51% yield. ^{1}H NMR (500 MHz, CDCl$_3$) δ 1.18 (d, J = 6.9 Hz, 6H), 2.44 (s, 3H), 2.83 (sept, J = 6.9 Hz, 1H), 3.57−3.64 (m, 2H), 3.95−4.05 (m, 2H), 5.29 (s, 1H), 7.05−7.15 (m, 4H), 7.23 (t, J = 8.3 Hz, 2H), 7.31 (t, J = 7.3 Hz, 2H), 7.37−7.40 (m, 2H), 7.46−7.52 (m, 3H), 8.03 (s, 1H).

2-[(4-Fluorobenzyl)(4-isopropylbenzyl)amino]-2-(7-methyl-2-oxo-1,2-dihydroquinolin-3-yl)acetonitrile (22): Following the Method D, the title compound was synthesized in 64% yield. ^{1}H NMR (500 MHz, CDCl$_3$) δ 1.18 (d, J = 6.9 Hz, 6H), 2.44 (s, 3H), 2.83 (sept, J = 6.9 Hz, 1H), 3.57−3.62 (m, 2H), 3.97−4.00 (m, 2H), 5.31 (s, 1H), 6.99 (t, J = 8.6 Hz, 1H), 7.08−7.14 (m, 4H), 7.35 (d, J = 8.1 Hz, 2H), 7.46−7.49 (m, 3H), 8.05 (s, 1H), 11.5 (s, 1H).

2-(Benzyl(4-isopropylbenzyl)amino)-2-(6-methyl-2-oxo-1,2-dihydroquinolin-3-yl)acetonitrile (23): Following the Method D, the title compound was synthesized in 73% yield. ^{1}H NMR (500 MHz, CDCl$_3$) δ 1.23 (d, J = 7.1 Hz, 6H), 2.59 (s, 3H), 2.89 (sept, J = 7.1 Hz, 1H), 3.44 (d, J = 13.5 Hz, 1H), 3.45 (d, J = 13.5 Hz, 1H), 3.86 (d, J = 13.2 Hz, 1H), 3.87 (d, J = 13.5 Hz, 1H), 5.10 (s, 1H), 7.03 (d, J = 8.6 Hz, 1H), 7.20 (d, J = 8.1 Hz, 1H), 7.29 (d, J = 8.1 Hz, 1H), 7.33−7.35 (m, 2H), 7.44 (dd, J = 1.7, 8.3 Hz, 1H), 7.76 (d, J = 8.3 Hz, 1H), 8.28−8.29 (m, 1H), 8.94(d, J = 2.5 Hz, 1H).

3-[1-((4-Fluorobenzyl)(4-isopropylbenzyl)amino)ethyl]-6-methylquinolin-2(1H)-one (24) (Method E): A mixture of *N*-(4-Fluorobenzyl)-1-(4-isopropylphenyl)methanamine (77 mg, 0.3 mmol), 3-(chloromethyl)-7-methylquinolin-2(1H)-one (80 mg, 0.3 mmol) and K$_2$CO$_3$ (124 mg, 0.9 mmol) in DMF (3.0 mL) was

stirred at 80 °C for 12 hrs. The mixture was added H$_2$O and extracted with EtOAc. The organic layers were washed with brine, dried over MgSO$_4$ and concentrated under vacuum. The residue was purified by column chromatography on SiO$_2$ gel (hexane-EtOAc 4:1 to 2:1) to afford the product (103 mg, 80 % yield). ^{1}H NMR (500 MHz, CDCl$_3$) δ 1.22 (d, J = 7.1 Hz, 6H), 1.45 (d, J = 7.1 Hz, 3H), 2.42 (s, 3H), 2.86 (sept, J = 7.1 Hz, 1H), 3.62−3.77 (m, 4H), 4.41 (q, J = 7.1 Hz, 1H), 6.96 (t, J = 7.8 Hz, 2H), 7.02−7.05 (m, 2H), 7.13 (d, J = 8.1 Hz, 2H), 7.32 (d, J = 8.1 Hz, 2H), 7.37−7.41 (m, 2H), 7.44 (d, J = 7.8 Hz, 2H), 7.79 (s, 1H), 10.8 (s, 1H).

3-[1-((4-Fluorobenzyl)(4-isopropylbenzyl)amino)pentyl]-7-methylquinolin-2(1H)-one (25): Following the Method E, the title compound was synthesized in 26% yield. ^{1}H NMR (500 MHz, CDCl$_3$) δ 0.83 (t, J = 7.1 Hz, 3H), 1,.19−1.27 (m, 9H), 1.35−1.44 (m, 1H), 1.78−1.85 (m, 1H), 2.00−2.08 (m, 1H), 2.42 (s, 3H), 2.87 (sept, J = 7.1 Hz, 1H), 3.41 (d, J = 13.7 Hz, 1H), 3.48 (d, J = 14.0 Hz, 1H), 3.80 (d, J =14.0 Hz, 1H), 3.86 (d, J = 13.7 Hz, 1H), 4.25 (t, J =7.6 Hz, 1H), 6.96 (t, J = 8.8 Hz, 2H), 7.04−7.05 (m, 2H), 7.15 (d, J = 8.1 Hz, 2H), 7.21−7.27 (m, 1H), 7.30−7.32 (m, 3H), 7.36−7.39 (m, 2H), 7.45 (d, J = 8.6 Hz, 1H), 7.58 (s, 1H), 10.6 (s, 1H); LRMS (DART$^+$): m/z: 485 [M+H]$^+$

7-Methyl-3-[2,2,2-trifluoro-1-((4-fluorobenzyl)(4-isopropylbenzyl)amino)ethyl]quinolin-2(1H)-one (26): Following the Method E, the title compound was synthesized in 69% yield. ^{1}H NMR (500 MHz, CDCl$_3$) δ 1.25 (d, J = 6.9 Hz, 3H), 1.26 (d, J = 6.9 Hz, 3H), 2.48 (s, 3H), 2.90 (sept, J = 6.9 Hz, 1H), 3.57−4.03 (m, 4H), 5.20 (q, J = 6.9 Hz, 1H), 7.00 (t, J = 8.8 Hz, 2H), 7.11−7.13 (m, 1H), 7.16−7.21 (m, 3H), 7.25 (s, 1H), 7.38 (d, J = 8.1 Hz, 2H), 7.45−7.47 (m, 2H), 7.52 (d, J = 8.1 Hz, 1H), 8.02 (s, 1H), 12.6 (s, 1H); LRMS (DART$^+$): m/z: 497 [M+H]$^+$

3-[((4-Fluorobenzyl)(4-isopropylbenzyl)amino)methyl]-7-methylquinolin-2(1H)-one (27): Following the Method E, the title compound was synthesized in 68% yield. ^{1}H NMR (500 MHz, CDCl$_3$) δ 1.22 (d, J = 6.8 Hz, 6H), 2.44 (s, 3H), 2.88 (sept, J = 6.8 Hz, 1H), 3.84−3.70 (m, 6H), 6.98−7.05 (m, 4H), 7.18 (d, J = 8.1 Hz, 2H), 7.46 (d, J = 8.1 Hz, 2H), 7.40−7.43 (m, 2H), 7.48 (d, J = 8.3 Hz, 1H), 8.01 (s, 1H), 10.5 (s, 1H); LRMS (DART$^+$): m/z: 429 [M+H]$^+$

3-[((4-(*tert*-Butyl)benzyl)(4-fluorobenzyl)amino)methyl]-6-methylquinolin-2(1H)-one (37): Following the Method E, the title compound was synthesized in 23% yield. ^{1}H NMR (500 MHz, CDCl$_3$) δ 1.30 (s, 9H), 2.43 (s, 3H), 3.66 (s, 6H), 7.00 (t, J = 8.6 Hz, 2H), 7.09 (d, J = 8.3 Hz, 1H), 7.20−7.29 (m, 1H), 7.33−7.43 (m, 7H), 8.01 (s, 1H), 9.69 (s, 1H); LRMS (DART$^+$): m/z: 443 [M+H]$^+$

3-[((4-(*tert*-Butyl)benzyl)(4-methoxybenzyl)amino)methyl]-6-methylquinolin-2(1H)-one (63): Following the Method D, the title compound was synthesized in 46% yield. ^{1}H NMR (500 MHz, CDCl$_3$) δ 1.30 (s, 9H), 2.43 (s, 3H), 3.63 (s, 2H), 3.65 (s, 4H), 3.79 (s, 3H), 6.86 (d, J = 8.6 Hz, 2H), 7.07−7.08 (m, 1H), 7.26−7.40 (m, 8H), 8.05 (s, 1H), 9.60 (s, 1H); LRMS (DART$^+$): m/z: 455 [M+H]$^+$

(S)-3-[((4-(*tert*-Butyl)benzyl)(1-(4-methoxyphenyl)ethyl)amino)methyl]-6-ethylquinolin-2(1H)-one (89): Following the Method E, the title compound was synthesized in 24% yield. ^{1}H NMR (500 MHz, CDCl$_3$) δ 1.28 (s, 9H), 1.31 (t, J = 7.6 Hz, 3H), 1.50 (d, J = 6.9 Hz, 3H), 2.73 (q, J = 7.6 Hz, 2H), 3.38−3.63 (m, 2H), 3.72−3.78 (m, 2H), 3.80 (s, 3H), 4.03 (q, J = 6.8 Hz, 1H), 6.89 (d, J = 8.8 Hz, 2H), 7.28−7.32 (m, 4H), 7.38−7.40 (m, 3H), 7.42 (d, J = 8.3 Hz, 2H), 8.05 (s, 1H), 11.7 (br.s, 1H); ^{13}C NMR (125 MHz, CDCl$_3$) δ 14.6, 15.8, 28.4, 31.3, 34.4, 47.6, 54.4, 55.2, 56.9, 113.4, 115.5, 120.2, 125.1, 125.9, 128.1, 128.9, 129.8, 131.7, 135.2, 135.3, 137.0, 137.1,

138.3, 149.5, 158.3, 163.8, HRMS (EI) *m/z* Calcd for $C_{32}H_{38}N_2O_2$ [M]$^+$ 482.2933, found 482.2926, [α] $_D^{30}$ = −107.5 (c = 0.50 in CHCl$_3$).

3-[((4-(*tert*-butyl)benzyl)(1-(3-chloro-4-methoxyphenyl)ethyl)amino)methyl]-6-methoxyquinolin-2(1*H*)-one (100): Following the Method E, the title compound was synthesized in 14% yield. ^{1}H NMR (500 MHz, CDCl$_3$) δ 1.28 (s, 9H), 1.49 (d, *J* = 6.9 Hz, 3H), 3.58 (d, *J* = 17.6 Hz, 1H), 3.64 (d, *J* = 14.2 Hz, 1H), 3.72 (d, *J* = 14.0 Hz, 1H), 3.80 (d, *J* = 17.6 Hz, 1H), 3.88 (s, 3H), 3.90 (s, 3H), 6.89 (d, *J* = 8.6 Hz, 1H), 7.01 (d, *J* = 2.7 Hz, 1H), 7.11 (dd, *J* = 2.7, 8.8 Hz, 1H), 7.32−7.39 (m, 6H), 7.51 (d, *J* = 2.0 Hz, 1H), 7.99 (s, 1H), 12.1 (br.s, 1H); ^{13}C NMR (125 MHz, CDCl$_3$) δ 14.2, 31.1, 31.3, 34.4, 47.6, 55.5, 55.7, 55.7, 56.1, 56.7, 108.6, 111.6, 116.9, 119.1, 120.7, 121.9, 125.2, 127.0, 128.1, 129.7, 131.8, 132.0, 136.5, 136.7, 149.7, 153.6, 155.0, 163.4; HRMS (EI) *m/z* Calcd for $C_{31}H_{35}ClN_2O_3$ [M]$^+$ 518.2336, found 518.2328.

6-Bromo-3-[((4-(*tert*-butyl)benzyl)(1-(4-(trifluoromethoxy)phenyl)ethyl)amino)methyl]-1,8-naphthyridin-2(1*H*)-one (118S): A mixture of *N*-(4-(*tert*-butyl)benzyl)-1-(4-(trifluoromethoxy)phenyl)ethan-1-amine (0.80 g, 2.28 mmol), 6-bromo-3-(bromomethyl)-1,8-naphthyridin-2(1*H*)-one (60% purity, 1.45 g, 2.74 mmol), DIPEA (442 mg, 3.42 mmol), and DMF (15 mL) was stirred at room temperature for 15 h. The mixture was diluted with water and extracted with EtOAc. The organic layer was washed with brine, dried over anhydrous MgSO$_4$, and concentrated in vacuo. The residue was purified by column chromatography (silica-gel, hexane/EtOAc=8/2 to 5/5, and NH silica-gel, Hexane/EtOAc=5/5 to 100%) to afford the product (480 mg, 36% yield) as a white amorphous powder. ^{1}H NMR (300 MHz, DMSO-*d$_6$*) δ 1.19 (s, 9H), 1.44 (d, *J*=6.8 Hz, 3H), 3.32 - 3.76 (m, 4H), 3.80 - 4.16 (m, 1H), 7.23 - 7.38 (m, 6H), 7.61 (d, *J*=8.7 Hz, 2H), 7.96 (s, 1H), 8.49 (dd, *J*=16.6, 2.3 Hz, 2H), 12.24 (s, 1H); LRMS (DART$^+$): m/z 588.2 [M+H]$^+$

3-[((4-(*tert*-Butyl)benzyl)(1-(4-(trifluoromethoxy)phenyl)ethyl)amino)methyl]-6-cyclopropyl-1,8-naphthyridin-2(1*H*)-one: A mixture of 6-bromo-3-(((4-(*tert*-butyl)benzyl)(1-(4-(trifluoromethoxy)phenyl)ethyl)amino)methyl)-1,8-naphthyridin-2(1*H*)-one (118S) (480 mg, 0.82 mmol), cyclopropyl boronic acid (210 mg, 2.45 mmol), Pd$_2$(dba)$_3$ (74.7 mg, 0.08 mmol), SPhos (67.0 mg, 0.16 mmol), Na$_2$CO$_3$ (432 mg, 4.08 mmol,), water (2 mL), and toluene (8 mL) was stirred at 120 °C for 1 h under microwave irradiation. The mixture was diluted with water and extracted with EtOAc. The organic layer was washed with brine, dried over anhydrous Na$_2$SO$_4$, and concentrated in vacuo. The residue was purified by column chromatography (silica gel, hexane/EtOAc=10/1to 50/50) to afford racemate of the product (270 mg, 60%). The racemate (153 mg) was purified by chiral HPLC (Column: CHIRALPAK AD-H(VA003) 20 mmID*250 mmL, 5 μm. Mobile phase: Hexane / Ethanol=600/400(v/v). Flow rate: 20 mL/min. Detection: UV 220 nm. Temperature: room temperature) to give **(−)**-isomer **(118)** (45 mg) as colorless solid (98.2 % e.e.) and **(+)**-isomer **(119)** (35 mg) as colorless solid (99.8 % e.e.).

(−)-3-[((4-(*tert*-Butyl)benzyl)(1-(4-(trifluoromethoxy)phenyl)ethyl)amino)methyl]-6-cyclopropyl-1,8-naphthyridin-2(1*H*)-one (118): Chiral analysis: Retention time was 14.0 min (Column: CHIRALPAK AD-H(UK216) 4.6 mmID*250 mmL, 5 mm, Mobile phase: Hexane / EtOH / Diethyamine=600/400/1(v/v/v), Flow rate: 1.0 mL/min. Detection: UV 220 nm. Temperature: 30 °C). ^{1}H NMR (500 MHz, CDCl$_3$) δ 0.76−0.80 (m, 2H), 1.03−1.08 (m, 2H), 1.28 (s, 9H), 1.49 (d, *J* = 6.9 Hz, 3H), 1.98−2.03 (m, 1H), 3.55 (d, *J* = 17.4 Hz, 1H), 3.62 (d,

J = 14.2 Hz, 1H), 3.70 (d, *J* = 13.9 Hz, 1H), 3.78 (d, *J* = 17. 4Hz, 1H), 4.05 (q, *J* = 6.8 Hz, 1H), 7.18 (d, *J* = 8.3 Hz, 2H), 7.33 (d, *J* = 8.6 Hz, 2H), 7.35 (d, *J* = 8.6 Hz, 2H), 7.49 (d,*J* = 8.8Hz, 2H), 7.52 (d, *J* = 1.7 Hz, 1H), 7.89 (s, 1H), 8.47 (s, 1H), 11.3 (br.s, 1H); ^{13}C NMR (125 MHz, CDCl$_3$) δ 8.60, 12.7, 14.2, 31.3, 34.4, 47.8, 54.8, 57.2, 114.9, 120.5, 125.3, 128.1, 129.0, 132.5, 134.0, 134.2, 134.3, 136.4, 141.8, 146.6, 148.0, 148.4, 149.9, 163.2; HRMS (FAB) *m/z* Calcd for $C_{32}H_{34}F_3N_3O_2$ [M+H]$^+$ 550.2681, found 550.2681; [α] $_D^{30}$ = −102.4 (c = 0.50 in CHCl$_3$).

(+)-3-[((4-(*tert*-Butyl)benzyl)(1-(4-(trifluoromethoxy)phenyl)ethyl)amino)methyl]-6-cyclopropyl-1,8-naphthyridin-2(1*H*)-one (119): Chiral analysis: Retention time was 10.1 min (Column: CHIRALPAK AD-H(UK216) 4.6 mmID*250 mmL, 5 mm, Mobile phase: Hexane / EtOH / Diethyamine=600/400/1(v/v/v), Flow rate: 1.0 mL/min. Detection: UV 220 nm. Temperature: 30°C). ^{1}H NMR (300 MHz, DMSO-*d$_6$*) δ 0.74−0.87 (m, 2H), 0.92−1.11 (m, 2H), 1.20 (s, 9H), 1.44 (d, *J* = 6.8 Hz, 3H), 2.01 (s, 1H), 3.33−3.75 (m, 4H), 3.96 (d, *J*=6.8 Hz. 1H), 7.26−7.35 (m, 6H), 7.59 (d, *J* = 8.7 Hz, 2H), 7.78 (d, *J* = 2.3 Hz, 1H), 7.92 (s, 1H), 8.31 (d, *J* = 2.3 Hz, 1H), 11.96 (s, 1H); LRMS (ESI): m/z 550.3 [M+H]$^+$; [α] $_D^{30}$ = 124.4(c = 0.50 in CHCl$_3$)

ASSOCIATED CONTENT

Supporting Information.
Details of experimental methods and additional information of characterization data for synthesized compounds. Transcription assay for **PA-49**, **89**, oseltamivir, and favipiravir. Binding mode of compounds of **89**, **100**, and **118** predicted by the docking simulation and their docking scores. Hemmagglutination titration assay and Influenza virus inhibitory activity of **100** and **118** against multiple strains. HPLC traces and NMR spectra for **89**, **100**, and **118**. PDB files for the complex structures of PA/**PA-49**, PA/**89**, PA/**100**, and PA/**108**. Molecular formula strings and *in vitro* biological activity (CSV). This material is available free of charge via the Internet at http://pubs.acs.org."

AUTHOR INFORMATION

Corresponding Authors

Satoshi Mizuta − *Center for Bioinformatics and Molecular Medicine, Graduate School of Biomedical Sciences, Nagasaki University, 1-14 Bunkyo, Nagasaki, 852-8521, Japan.* E-mail, s-mizuta@nagasaki-u.ac.jp

Ken Watanabe − *Department of Lifestyle Design, Faculty of Human Ecology, Yasuda Women's University, 6-13-1 Yasuhigashi, Asaminami ward, Hiroshima 731-0153, Japan.* E-mail, watanabe-k@yasuda-u.ac.jp

Authors

Hiroki Otaki − Center for Bioinformatics and Molecular Medicine, Graduate School of Biomedical Sciences, Nagasaki University, 1-14 Bunkyo, Nagasaki, 852-8521, Japan
Takeshi Ishikawa − Department of Chemistry, Biotechnology, and Chemical Engineering, Graduate School of Science and Engineering, Kagoshima University, 1-21-40 Korimoto, Kagoshima 890-0065, Japan
Juliann Nzembi Makau − Center for Virus Research, Kenya Medical Research Institute, 54840-00200, Nairobi, Kenya
Tomoko Yamaguchi − Center for Bioinformatics and Molecular Medicine, Graduate School of Biomedical Sciences, Nagasaki University, 1-14 Bunkyo, Nagasaki, 852-8521, Japan

Takuya Fujimoto − Chemistry, Discovery Science, Axcelead Drug Discovery Partners, Inc., 26-1, Muraoka-Higashi 2-chome, Fujisawa, Kanagawa 251-0012, Japan

Nobuyuki Takakura − Chemistry, Discovery Science, Axcelead Drug Discovery Partners, Inc., 26-1, Muraoka-Higashi 2-chome, Fujisawa, Kanagawa 251-0012, Japan

Nobuki Sakauchi − Chemistry, Discovery Science, Axcelead Drug Discovery Partners, Inc., 26-1, Muraoka-Higashi 2-chome, Fujisawa, Kanagawa 251-0012, Japan

Shuji Kitamura − Chemistry, Discovery Science, Axcelead Drug Discovery Partners, Inc., 26-1, Muraoka-Higashi 2-chome, Fujisawa, Kanagawa 251-0012, Japan

Hikaru Nono − School of Medicine, Nagasaki University, 1-12-4 Sakamoto, Nagasaki, 852-8523, Japan

Ryota Nishi − School of Medicine, Nagasaki University, 1-12-4 Sakamoto,, Nagasaki, 852-8523, Japan

Yoshimasa Tanaka − Center for Medical Innovation, Nagasaki University, 1-7-1 Sakamoto, Nagasaki, 852-8521, Japan

Kohsuke Takeda − Department of Cell Regulation, Graduate School of Biomedical Sciences, Nagasaki University, 1-14 Bunkyo, Nagasaki, 852-8521, Japan

Noriyuki Nishida − Department of Molecular Microbiology and Immunology, Graduate School of Biomedical Sciences, Nagasaki University, 1-12-4 Sakamoto, Nagasaki, 852-8523, Japan

Notes

The authors declare no competing financial interest.

ABBREVIATIONS USED

AcOH, acetic acid; AIBN, 2,2'-azodiisobutyronitrile; SBDD, structure-based drug discovery; BXA, baloxavir acid; BXM, baloxavir marboxil; CC_{50}, 50% cytotoxic concentration; CV, crystal violet; DART, direct analysis in real time; DIPEA, $N,$-ethyldiisopropylamine; DMA, N, N-dimethylacetamide; DMF, N,N-dimethylacetamide; DMSO, dimethy sulfoxide; EC_{50}, 50% effective concentration; EHT; extended Hückel theory; Et_3N, triethylamine; EtOAc, ethyl acetate; EtOH, ethanol; FBS, fetal bovine serum; GFP, green fluorescent protein; HPLC, high performance liquid chromatography, HRMS, high resolution mass spectrum; LRMS, low resolution mass spectrum ; MDCK, Madin–Darby canine kidney; MeCN, acetnitrile; MEM, minimum essential medium; MeOH, methanol; MOE, Molecular Operating Environment; NBS, N-bromosuccinimide; NMR: nuclear magnetic resonance ; TLC, thin-layer chromatography; $Ti(OiPr)_4$, titanium(IV) isopropoxide; TFA, trifluoroacetic acid; THF, tetrahydrofuran; TMSCN, trimethylsilyl cyanide; $Pd_2(dba)_3$, tris(dibenzylideneacetone)dipalladium(0); RNA, ribonucleic acid; RdRp, RNA-dependent RNA polymerase; SARs, structure-activity relationships; SPhos, 2-dicyclohexylphosphino-2',6'-dimethoxybiphenyl; WHO, World Health Organization; NA, neuraminidase.

REFERENCES

(1) Dunning, J.; Baillie, J. K.; Cao, B.; Hayden, F. G. International Severe Acute, R. Emerging Infection, C. Antiviral combinations for severe influenza. *Lancet Infect. Dis*. **2014**, *14*, 1259−1270.

(2) Mills, C. E.; Robins, J. M.; Lipsitch, M. Transmissibility of 1918 pandemic influenza. *Nature* **2004**, *432*, 904−906.

(3) Steel, J.; Lowen, A. C. Influenza A virus reassortment: Influenza pathogenesis and control-Vol I, Compans, W. R.; Oldstone, M. B. A., Eds.; Springer: Cham, Switzerland, **2014**, *385*, 377−401.

(4) Liu, Sun, H.; Xiao, Y.; Liu, J.; Wang, D.; Li, F.; Wang, C.; Li, C.; Zhu, J.; Song, J.; Sun, H.; Jiang, Z.; Liu, L.; Zhang, X.; Wei, K.; Hou, D.; Pu, J.; Sun, Y.; Tong, Q.; Bi, Y.; Chang K. C.; Liu, S.; Gao, G. F.; Liu, J. **Prevalent Eurasian avian-like H1N1 swine influenza virus with 2009 pandemic viral genes facilitating human infection.** *Proc. Natl. Acad. Sci. USA*, **2020**, *117*, 17204−17210.

(5) Clercq, E. D. Antiviral agents active against influenza A viruses. *Nat. Rev Drug Discov.* **2006**, *5*, 1015−1025.

(6) Hayden, F.G.; Sugaya, N.; Hirotsu, N.; Lee, N.; de Jong, M. D.; Hurt, A. C.; Ishida, T.; Sekino, H.; Yamada, K.; Portsmouth, S.; Kawaguchi, K.; Shishido, T.; Arai, M.; Tsuchiya, K.; Uehara, T.; Watanabe, A.; for the Baloxavir Marboxil Investigators Group. Baloxavir marboxil for uncomplicated influenza in adults and adolescents. *N. Engl. J. Med.* **2018**, *379*, 913–923.

(7) Dehyde, V. M.; Xu, X.; Bright, R. A.; Shaw, M.; Smith, C. B.; Zhang, Y.; Shu, Y.; Gubareva, L. V.; Cox, N. J.; Klimov, A. I. Surveillance of resistance to adamantanes among influenza A(H3N2) and A(H1N1) viruses isolated worldwide. *J. infect. Dis.* **2007**, *196*, 249–257.

(8) Furuse, Y.; Suzuki, A.; Oshitani, H. Large-Scale Sequence Analysis of M Gene of Influenza A Viruses from Different Species: Mechanisms for Emergence and Spread of Amantadine Resistance. *Antimicrob. Agents Chemother.* **2009**, *53*, 4457–4463.

(9) Jalily, P. H.; Duncan, M. C.; Fedida, D.; Wang, J.; Tietjen, I. Put a cork in it: plugging the M2 viral ion channel to sink influenza. *Antiviral Res.* **2020**, 104780.

(10) Watanabe, T.; Kawaoka, T. Influenza virus-host interactomes as a basis for antiviral drug development. *Curr. Opin. Virol.* **2015**, *14*, 71–78.

(11) Fiore, A. E.; Fry, A.; Shay, D.; Gubareva, L.; Bresee, J. S.; Uyeki, T. M. Antiviral agents for the treatment and chemoprophylaxis of influenza: recommendations of the Advisory Committee on Immunization Practices (ACIP). *Morbidity Mortality Wkly. Rep.* **2011**, *60*, 1−24.

(12) Yamashita, M.; Krystal, M.; Palese, P. Comparison of the three large polymerase proteins of influenza A, B, and C viruses. *Virology* **1989**, *171*, 458–466.

(13) Obayashi, E.; Yoshida, Y.; Kawai, F.; Shibayama, N.; Kawagushi, A.; Nagata, J.; Tame, J .R.; Park, S. Y. The structure basis for an essential subunit interaction in influenza virus RNA polymerase. *Nature* **2008**, *454*, 1127−1131.

(14) Digarad, P.; Blok, V. C.; Inglis, S. C. Complex formation between influenza virus polymerase proteins expressed in Xenopus oocytes. *Virology* **1989**, *171*, 162−169.

(15) Toyoda, T.; Adyshev, D. M.; Kobayashi, M.; Iwata, A.; Ishihama, A. Molecular assembly of the influenza virus RNA polymerase: de-

termination of the subunit-subunit contact sites. *J. Gen. Virol.* **1996**, *77*, 2149–2157.

(16) Hara, K.; Schmidt, F. I.; Crow, M.; Brownlee, G. G. Amino acid residues in the N-terminal region of the subunit of influenza A virus RNA polymerase play a critical role in protein stability, endonuclease activity, cap binding, and virion RNA promoter binding. *J. Virol.* **2006**, *80*, 7789–7798.

(17) Li, M. L.; Rao, P.; Krug, R. M. The active sites of the influenza cap-dependent endonuclease are on different polymerase subunits. *EMBO J.* **2001**, *20*, 2078–2086.

(18) Poch, O.; Sauvagent, I.; Delaure, M.; Tordo, N. Identification of four conserved motifs among the RNA-dependent polymerase encoding elements. *EMBO J.* **1989**, *8*, 3867–3874.

(19) Guilligay, D.; Tarendeau, F.; Resa-Infante, P.; Coloma, R.; Crepin, T.; Sehr, P.; Lewis, J.; Ruigrok, R. W. H.; Ortin, J.; Hart, D. J.; Cusack, S. The structural basis for cap binding by influenza virus polymerase subunit PB2. *Nature Struct. Mol. Biol.* **2008**, *15*, 500–506.

(20) Stevaert, A.; Naesens, L.; The influenza virus polymerase complex: an update on its structure, functions, and significance for antiviral drug design. *Med. Res. Rev.* **2016**, *36*, 1127–1173.

(21) Hayden, F.G.; Shindo, N. Influenza virus polymerase inhibitors in clinical development. *Curr. Opin. Infect. Dis.* **2019**, *32*, 176−186.

(22) Omoto, S.; Speranzini, V.; Hashimoto, T.; Noshi, T.; Yamaguchi, H.; Kawai, M.; Kawaguchi, K.; Uehara, T.; Shishido, T.; Naito, A.; Cusack, S. Characterization of influenza virus variants induced by treatment with the endonuclease inhibitor baloxavir marboxil. *Sci. Rep.* **2018**, 8:9633. doi:10.1038/s41598-018-27890-4.

(23) Goldhill, D. H.; Te Velthuis, A. J. W.; Fletcher, R. A.; Langat. P.; Zambon, M.; Lackenby, A.; Varclay, W. S. The mechanism of resistance to favipiravir in influenza. *Proc. Natl. Acad. Sci. USA*, **2018**, *115*, 11613−11618.

(24) Manz, B.; Götz, V.; Wunderlich, K.; Eisel, J.; Kirchmair, J.; Stech, J.; Stech, O.; Chase, G.; Frank, R.; Schwemmle, M. Disruption of the viral polymerase complex assembly as a novel approach to attenuate influenza A virus. *J. Biol. Chem.* **2011**, 286, 8414–8424.

(25) Deng, T.; Sharps, J.; Fodor, E.; Brownlee, G. G. *In vitro* assembly of PB2 with a PB1-PA dimer supports a new model of assembly of influenza A virus polymerase subunits into a functional trimeric complex. *J. Virol.* **2005**, *79*, 8669−8674.

(26) He, X.; Zhou, J.; Bartlam, M.; Zhang, R.; Ma, J.; Lou, Z.; Li, X.; Li, J.; Joachimiak, A.; Zeng, Z.; Ge, R.; Rao, Z.; Liu, Y. Crystal structure of the polymerase PAC-PB1N complex from an avian influenza H5N1 virus. *Nature* **2008**, *454*, 1123–1126.

(27) Fukuoka, M.; Minakuchi, M.; Kawaguchi, A.; Nagata, K.; Kamatari, Y. O.; Kuwata, K. Structure-based discovery of anti-influenza virus A compounds among medicines. *Biochim. Biophys. Acta* **2012**, 1820, 90−95.

(28) Massari, S.; Nannetti, G.; Goracci, L.; Sancineto, L.; Muratore, G.; Sabatini, S.; Manfroni, G.; Mercorelli, B.; Cecchetti, V.; Facchini, M.; Palu, G.; Cruciani, G.; Loregian, A.; Taba`rrini, O. Structural investigation of cycloheptathiophene-3-carboxamide derivatives targeting influenza virus polymerase assembly. *J. Med. Chem.* **2013**, *56*, 10118−10131.

(29) Desantis, J.; Nannetti, G.; Massari, S.; Barreca, M. L. Manfroni, G.; Cecchetti, V.; Palù, G.; Goracci, L.; Loregian, A.; Tabarrini, O. Exploring the cycloheptathiophene-3-carboxamide scaffold to disrupt the interactions of the influenza polymerase subunits and obtain potent anti-influenza activity. *Eur. J. Med. Chem.* **2017**, *138*, 128−139.

(30) Trist, I. M. L.; Nannetti, G.; Tintori, C.; Fallacara, A. L.; Deodato, D.; Mercorelli, B.; Palù, G.; Wijtmans, M.; Gospodova, T.; Edink, E.; Verheij, M.; de Esch, I.; Viteva, L.; Loregian, A.; Botta, M. 4,6-Diphenylpyridines as promising novel anti-influenza agents targeting the PA−PB1 protein−protein interaction: structure−activity relationships exploration with the aid of molecular modeling. *J. Med. Chem.* **2016**, *59*, 2688−2703.

(31) Yuan, S.; Chu, H.; Zhao, H.; Zhan, K.; Sing, K.; Chow, B. K. C.; Kao, R. Y. T.; Zhou, J.; Zhen, B.J. Identification of a small-molecule inhibitor of influenza virus via disrupting the subunits interaction of the viral polymerase. *Antiviral Res.* **2016**, *125*, 34–42.

(32) Zhang, J.; Hu, Y.; Wu, N.; Wang, J. Discovery of influenza polymerase PA–PB1 interaction inhibitors using an *in vitro* split luciferase complementation-based assay. *ACS Chem. Biol.* **2020**, *15*, 74–82.

(33) Zhan, J.; Hu, Y.; Foley, C.; Wang, Y.; Musharrafieh, R.; Xu, S.; Zhang, Y.; Ma, C.; Hulme, C.; Wang, J. Exploring Ugi-azide four component reaction products for broad-spectrum influenza antivirals with a high genetic barrier to drug resistance. *Sci. Rep.* **2018**, 8:4653. doi:10.1038/s41598-018-22875-9.

(34) Hejdánek, J.; Radilová, K.; Pachl, P.; Hodek, J.; Machara, A.; Wever, J.; Řezáčová, P.; Kovalinka, J.; Kožíšek, M. Structural characterization of the interaction between the C-terminal domain of the influenza polymerase PA subunit and an optimized small peptide inhibitor. *Antivir. Res.* **2021**, *185*, 104971.doi:10.1016/j.antiviral.2020.104971.

(35) Watanabe, K.; Ishikawa, T.; Otaki, H.; Mizuta, S.; Hamada, T.; Nakagaki, T.; Ishibashi, D.; Urata, S.; Yasuda, J.; Tanaka, Y.; Nishida, N. Structure-based drug discovery for combating influenza virus by targeting the PA–PB1 interaction. *Sci. Rep.* **2017**, *7*, 9500.doi:10.1038/s41598-017-10021-w.

(36) Bazine, I.; Cheraiet, Z.; Bensegueni, R.; Bensouici, C.; Boukhari, A. Synthesis, antioxidant and anticholinesterase activities of novel quinoline-aminophosphonate derivatives. *J. Heterocyclic Chem.* **2020**. *57*, 3139−2149.

(37) Abonia, R.; Gutiérrez, L.; Insuasty, B.; Quiroga, J.; Laali, K. K.; Zhao. C.; Borosky, L. G.; Horwitz, M. S.; Bunge, D. S. Catalyst-free assembly of giant tris(heteroaryl)methanes: synthesis of novel pharmacophoric triads and model sterically crowded tris(heteroaryl/aryl)methyl cation salts. *Beilstein J. Org. Chem.* **2019**, *15*, 642−654.

(38) Katsikis, P. D.; Kinney, W. A.; Almond, H. R.; Khan, N. Novel PI3K p110 inhibitors and methods of use thereof, WO 2013090725 A1, June 20, **2013**.

(39) Xing, L.; Chen, C.; Zhu, R.; Zhang, B.; Wang, X. Self-modulated highly chemoselective direct-reductive-amination (DRA) of benzaldehydes straightforward to *N*-monosubstituted benzylamine hydrochlorides. *Tetrahedron* **2008***, 64*, 11783- 11788.

(40) Podyacheva, E.; Afanasyev, O. I.; Tsygankov, A. A.; Makarova, M.; Chusov, D. Hitchhiker's guide to reductive amination. *Synthesis* **2019**, *51*, 2667-2677.

(41) Heydari, A.; Khaksar, S.; Tajbakhsh, M. Trifluoroethanol as a metal-free, homogeneous and recyclable medium for the efficient one-pot synthesis of α-amino nitriles andα-amino phosphonates. *Tetrahedron Letters* **2009**, *50*, 77−80.

(42) Musiol, R. An overview of quinoline as a privileged scaffold in cancer drug discovery. *Expert Opin. Drug Discov.* **2017**, 12, 583−597.

(43) Magedov, I. V.; Manpadi, M.; Ogasawara, M. A.; Dhawan, A. S.; Rogelj, S.; Van Slambrouck, S.; Steelant, W. F. A.; Evdokimov, N. M.; Uglinskii, P. Y.; Elias, E. M.; Knee, E. J.; Tongwa, P.; Antipin, M. Y.; Kornienko, A. Structural simplification of bioactive natural products with multicomponent synthesis. 2. antiproliferative and antitubulin activities of pyrano[3,2-c]pyridones and pyrano[3,2-c]quinolones. *J. Med. Chem.* **2008**, *51*, 2561−70.

(44) Charyasriwong, S.; Watanabe, K; Rahmasari, R.; Matsunaga, A.; Haruyama, T.; Kobayashi, N. *In vitro* evaluation of synergistic inhibitory effects of neuraminidase inhibitors and methylglyoxal against influenza virus infection. *Arch. Med. Res.* **2015**, *46*, 8–16.

(45) Bohm, H. J.; Flohr, A.; Stahl, M. Scaffold hopping. *Drug Discov. Today Technol.* **2004**, *1*, 217−224.

(46) Mizuta, S.; Makau, J. N.; Kitagaw, A.; Kitamura, K.; Otaki, H.; Nishi, K.; Watanabe, K. Synthesis of trifluoromethyl-α,β-unsaturated lactones and pyrazolinones and discovery of influenza virus polymerase inhibitors. *ChemMedChem* **2018**, *13*, 2390 – 2399.

(47) Liu, H.; Yao, X. Molecular basis of the interaction for an essential subunit PA–PB1 in influenza virus RNA polymerase: insights from molecular dynamics simulation and free energy calculation. *Mol. Pharmaceutics* **2010**, *7*, 75−85.

(48) Molecular Operating Environment (MOE), 2019.01; Chemical Computing Group ULC, 1010 Sherbrooke St. West, Suite #910, Montreal, QC, Canada, H3A 2R7, 2020.

(49) Makau, N. J.; Watanabe, K.; Ishikawa, T.; Mizuta, S.; Hamada, T.; Kobayashi, N.; Nishida, N. Identification of small molecule inhibitors for influenza A virus using *in silico* and *in vitro* approaches. *PLoS ONE* **2017**,*12*: e0173582.

(50) Ozawa, M.; Fujii, K.; Muramoto, Y.; Yamada, S.; Yamayoshi, S.; Takada, A.; Goto, H.; Horimoto, T.; Kawaoka, Y. Contributions of two nuclear localization signals of influenza A virus nucleoprotein to viral replication. *J. Virol.* **2007**, *81*, 30–41.

(51) Ponder, J. W.; Case, D. A. Force fields for protein simulations. *In Adv. Protein Chem.* **2003**, *66*, 27–85.

(52) Gerber, P. R.; Müller, K. MAB, a generally applicable molecular force field for structure modelling in medicinal chemistry. J. Comput. Aided Mol. Des. **1995**, *9*, 251-268.

(53) Corbeil, C. R.; Williams, C. I.; Labute, P., Variability in docking success rates due to dataset preparation. *J. Comput. Aided Mol. Des.* **2012,** *26*, 775-786.
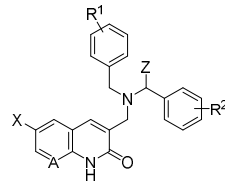
Table of Contents Graphic
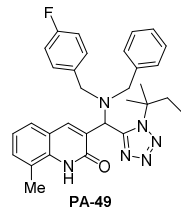
PA-49

EC$_{50}$ = 0.57 μM
CC$_{50}$ = > 83 μM
SI > 146

102 analogues

optimization

quinolinone
derivatives

EC$_{50}$ = ≥ 0.061 μM
CC$_{50}$ = > 10 μM
SI > 148

1,8-naphthyridinone
derivatives (A=N)

EC$_{50}$ = ≥ 0.077 μM
CC$_{50}$ = > 10 μM
SI > 130